CellPress

Cell Host & Microbe
Article

NRAV, a Long Noncoding RNA, Modulates Antiviral Responses through Suppression of Interferon-Stimulated Gene Transcription

Jing Ouyang,[1] Xiaomei Zhu,[1,2] Yuhai Chen,[1] Haitao Wei,[1] Qinghuang Chen,[1,3] Xiaojuan Chi,[3] Baomin Qi,[3] Lianfeng Zhang,[4] Yi Zhao,[5] George Fu Gao,[1] Guoshun Wang,[6] and Ji-Long Chen[1,3,*]

[1]CAS Key Laboratory of Pathogenic Microbiology and Immunology, Institute of Microbiology, Chinese Academy of Sciences, Beijing 100101, China

[2]School of Life Sciences, Anhui University, Hefei 230601, China

[3]College of Animal Sciences, Fujian Agriculture and Forestry University, Fuzhou 350002, China

[4]Institute of Laboratory Animal Science, Chinese Academy of Medical Sciences & Comparative Medical Center, Beijing 100021, China

[5]Key Laboratory of Intelligent Information Processing, Institute of Computing Technology, Chinese Academy of Sciences, Beijing 100190, China

[6]Gene Therapy Program, Departments of Microbiology and Immunology, Medicine and Genetics, Louisiana State University Health Sciences Center, New Orleans, LA 70112, USA

*Correspondence: chenjl@im.ac.cn

http://dx.doi.org/10.1016/j.chom.2014.10.001

SUMMARY

Long noncoding RNAs (lncRNAs) modulate various biological processes, but their role in host antiviral responses is largely unknown. Here we identify a lncRNA as a key regulator of antiviral innate immunity. Following from the observation that a lncRNA that we call *n*egative *r*egulator of *a*ntiviral response (NRAV) was dramatically downregulated during infection with several viruses, we ectopically expressed NRAV in human cells or transgenic mice and found that it significantly promotes influenza A virus (IAV) replication and virulence. Conversely, silencing NRAV suppressed IAV replication and virus production, suggesting that reduction of NRAV is part of the host antiviral innate immune response to virus infection. NRAV negatively regulates the initial transcription of multiple critical interferon-stimulated genes (ISGs), including IFITM3 and MxA, by affecting histone modification of these genes. Our results provide evidence for a lncRNA in modulating the antiviral interferon response.

INTRODUCTION

Thousands of lncRNAs are pervasively transcribed in mammalian cells. Accumulating data indicate that they are an important class of regulatory RNAs in a variety of cellular processes (Mercer et al., 2009). To serve the function of signaling, decoying, scaffolding, or guiding, lncRNAs employ their motifs to interact with other molecules (Guttman and Rinn, 2012; Wang and Chang, 2011). Most recently, three lncRNAs (murine NeST, human THRIL, and NEAT1) are shown to regulate the innate immunity by modulating the transcription of IFN-γ, TNF-α, and IL8, respectively (Cullen, 2013; Gomez et al., 2013; Imamura et al., 2014; Li et al., 2014). In addition, mouse lincRNA-Cox2 plays a central role in control of the Pam3CSK4-induced inflammatory response (Carpenter et al., 2013). Whole transcriptome studies have also demonstrated the differential expression of lncRNAs in SARS coronavirus-infected mice (Peng et al., 2010) and enterovirus 71-infected RD cells (Yin et al., 2013), suggesting the functional involvement of lncRNAs in antiviral immunity. Interestingly, several lncRNAs have been shown to modulate viral infection. For example, 7SL and NEAT1 are evidenced to interfere with the HIV-1 virion package and posttranscriptional expression (Wang et al., 2007; Zhang et al., 2013). lncRNA VIN can facilitate influenza A virus (IAV) propagation (Winterling et al., 2014). Despite these progresses, the specific functions of these lncRNAs in the host defense process remain incompletely characterized.

IAV infection poses a significant threat to global health (Mänz et al., 2013), but the mechanisms underlying IAV-host interaction are still elusive. Host anti-IAV response is initiated by the recognition of viral components by pathogen recognition receptors (PRRs), such as retinoic acid-inducible gene I (RIG-I), melanoma differentiation factor 5 (MDA5), and toll-like receptor 3 (TLR3). Through the signaling cascade downstream the stimulated receptors, transcription factors including IRF3/7 and NF-κB are activated. Type I and III interferons (IFNs) are then rapidly produced, which induce the synthesis of hundreds of antiviral proteins encoded by IFN-stimulated genes (ISGs). Consequently, the accumulation of ISG proteins in cytosol, including the well-known IFN-induced protein with tetratricopeptide repeats IFIT2, IFIT3 (Fensterl et al., 2012; Liu et al., 2011), IFN-induced transmembrane protein 3 (IFITM3) (Everitt et al., 2012), and myxovirus resistance 1 (human MxA or mouse Mx1) (Mänz et al., 2013), provides antiviral protection through multiple mechanisms. Importantly, modulation of anti-IAV immunity epigenetically has emerged to be a critical mechanism. After the activation of transcription factors, a transcriptional regulation cascade is triggered (Smale, 2012). The cascade includes

multiple waves of transcriptional activation and inhibition controlled by a complex network. First of all, regulations of promoter activity and chromatin structure are essential steps for the transcription initiation. For example, the activation of the promoters of immune genes *ifit2*, *ifit3*, and *mx1* requires nucleosome remodeling through SWItch/Sucrose NonFermentable (SWI/SNF) complexes and histone modifications (H3K4me3 or H3K9/K14ac) (Ramirez-Carrozzi et al., 2009). IFN-γ promoter is reported to be upregulated by lncRNA NeST, which binds with H3K4 methylase complex component WDR5 to alter histone methylation levels (Gomez et al., 2013). In addition, the mRNA maturation and stabilization are also critical posttranscriptional regulation steps. Heterogeneous nuclear ribonucleoproteins (hnRNPs) regulate gene transcription and subsequent modification of the newly synthesized RNA (pre-mRNA) in nucleus. Recent studies have shown that hnRNP L and hnRNP A/B are associated with the induction of immunity genes TNF-α and CCL5 through interaction with lncRNA THRIL and lincRNA-Cox2, respectively (Carpenter et al., 2013; Li et al., 2014). These data suggest that additional coregulators are required for transcriptional activation/inhibition of innate immunity genes.

In this study, genome-wide profiling of lncRNA expression identified a human lncRNA, designated NRAV, that played a critical role in anti-IAV infection. In vitro and in vivo data showed that NRAV functioned as a negative regulator in the host antiviral immunity by repression of ISG production through strict control of the transcription rate. Furthermore, we found that NRAV regulated the expression of MxA and IFITM3, likely through affecting histone modification of their genes. These results reveal a layer of the regulation of host innate defense during the IAV infection.

RESULTS

Human NRAV Is Identified as a lncRNA Controlling Virus Infection

To investigate the roles of host lncRNAs in IAV infection, genome-wide lncRNA microarrays were performed of human alveolar epithelial cells (A549) infected with or without influenza virus A/WSN/33 (H1N1) for 12 hr. A total of 494 upregulated and 413 downregulated lncRNAs following the viral infection were detected (fold change >2) and clustered (Figure 1A, left). Nine lncRNAs were selected as candidates after an in silico screen (see Supplemental Information available online) and confirmation by RT-PCR (Figure 1A, right).

To identify the functional lncRNAs, viral activity screening was performed (Figures S1A and S1B). lncRNA NRAV was found to affect the virus replication most significantly, and thus it was chosen for in-depth study. The human lncRNA gene *nrav* (LOC100506668, uc001tyk, also named as *dynll1-as1*) is located on chromosome 12q24.31, overlapping with the antisense strand of dynein light chain coding gene *dynll1* within intron 1 (Figure 1B). No protein-coding potential was found in NRAV by analysis using ORF Finder (NCBI), coding potential calculator (score is −0.743) (Figure S1C), and PhyloCSF (score is −3452) (Lin et al., 2011). Using polysome analysis, we further observed that NRAV displayed different distribution patterns in sucrose gradient fractions as compared with control protein-coding mRNA of GAPDH that locates in the same fractions as polysome, demonstrating the noncoding potential of NRAV (Figures S1D and S1E). Importantly, both qRT-PCR and northern blotting confirmed that NRAV expression was markedly reduced in IAV-infected A549 cells (Figures 1C and 1D). Northern blot analysis using a specific probe (793 nt) demonstrated that the major form of human NRAV was the transcript of approximately 1,200 nt (Figure 1D). Consistently, determination of 5′ and 3′ ends of NRAV by RACE studies revealed that NRAV transcript is exactly 1,176 nt and contains a polyadenylated (12 As) tail (Figures 1E and S1F; Table S1).

Furthermore, we observed that NRAV was downregulated in a virus dose- and infection time-dependent manner (Figure 1F). Interestingly, NRAV was expressed in various human cell lines, and its expression was dramatically reduced after IAV infection in all examined cell lines susceptible to the infection, but not in cell lines (HeLa, HepG2) less permissive to IAV replication (Figure 1G). Surprisingly, NRAV was also significantly downregulated by infections of several other viruses, including a negative ssRNA virus Sendai virus (SeV), a dsRNA virus Muscovy Duck Reovirus (MDRV), and a DNA virus herpes simplex virus (HSV) (Figures 1H and 1I). In contrast, NRAV levels were not affected by pseudovirus transduction, LPS treatment, etoposide stimulation, or serum withdrawal (Figures S1G–S1J). Together, these experiments demonstrate that reduction of NRAV level is associated with viral infection.

In addition, we identified NRAV homolog-coding sequences in monkey and mouse genomes through Blast (NCBI) in silico analysis. However, we only detected NRAV homolog transcript in monkey Vero cells, but not in mouse cells by RT-PCR (Figures S1K and S1L). These results suggest that the *nrav* gene may be conserved but evolved to be differentially regulated.

Altering NRAV Expression Has Profound Effects on IAV Replication in Human Cells

To further determine the functionality of NRAV in IAV infection, we generated A549 and 293T cell lines stably expressing whole length of the human NRAV or specific shRNAs targeting NRAV using the retroviral vectors or shRNA-based lentivectors (Figures 2A, S2A, and S2B). Although IAV infection reduced the endogenous NRAV expression, it had no significant effects on the ectopically expressed NRAV and could not diminish the difference of NRAV expression between sh-Luc control cells and NRAV knockdown cells (Figure 2B). Strikingly, both the virus growth kinetics measured by haemagglutination assay and the virus titers determined by plaque-forming test showed that forced expression of NRAV significantly promoted the viral replication, while disruption of NRAV expression consistently impaired the virus reproduction in A549 cells (Figures 2C–2E). The sh-NRAV-1 cells with lower NRAV expression were used in further studies. Similar results were obtained from NRAV overexpression and knockdown in 293T cells (Figure S2C). The increased virus titers in supernatant from NRAV-overexpressing cells were further confirmed by western blotting using an antibody against the IAV hemagglutinin (HA) (Figures S2D and S2E). Because IAV infection caused a marked decrease in NRAV expression in A549 cells, we determined whether NRAV levels in NRAV-knockdown cells were lower than those in the control cells during IAV infection. Indeed, the knockdown cells showed clearly low levels of NRAV compared with the controls (Figure 2F). However, the DYNLL1 levels were not affected by

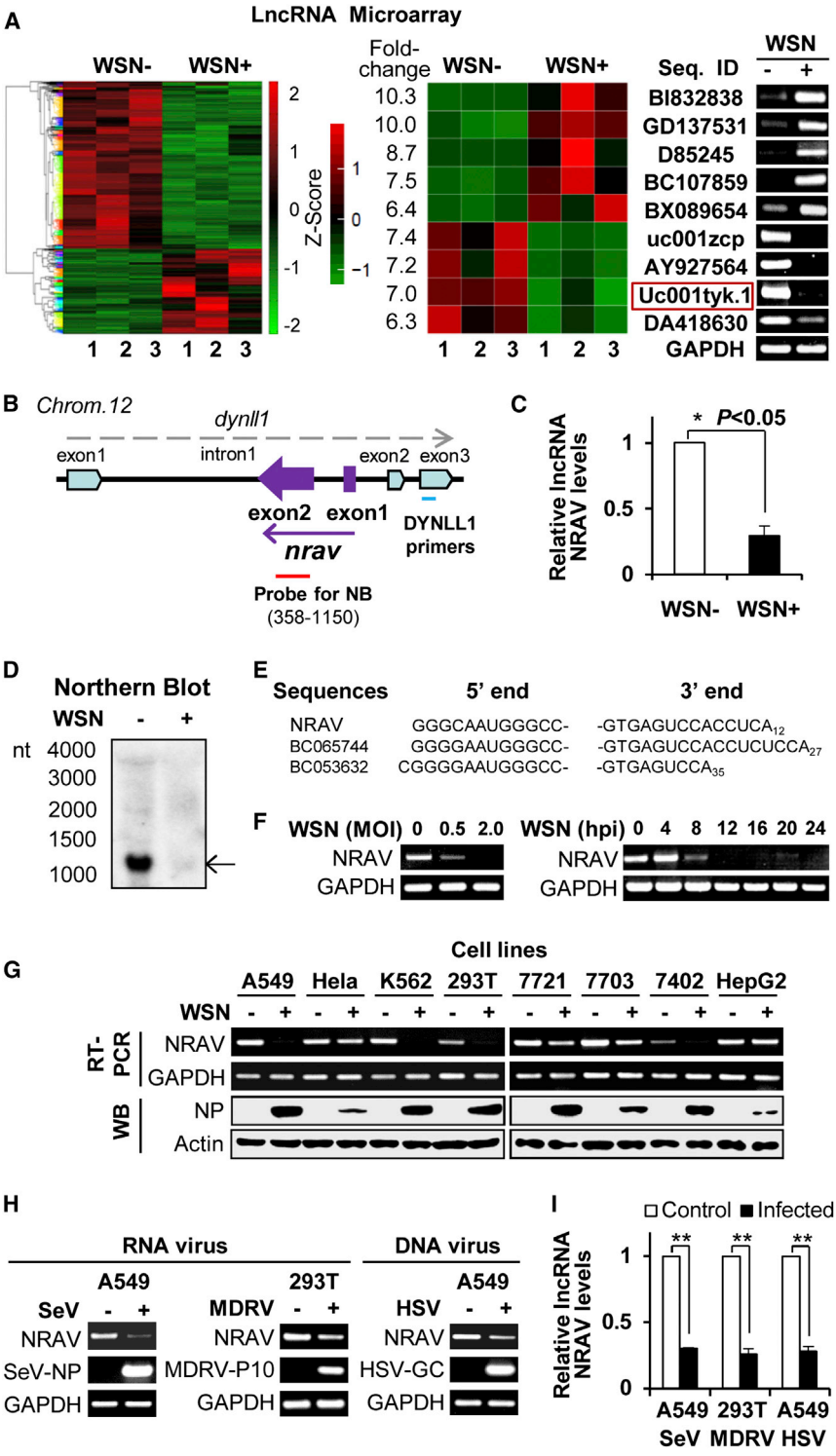

Figure 1. Human NRAV Is Identified as a lncRNA Involved in Virus Infection

(A) Microarray analysis revealed 494 upregulated and 413 downregulated lncRNAs in IAV-infected A549 cells compared to control (n = 3; fold change > 2.0; $p < 0.05$) (left). Cells infected with WSN were collected 12 hr postinfection (hpi). The RNA quantitation is shown as centered and scaled log2 data in heatmaps. The differential expressions of 9 selected lncRNAs were confirmed by RT-PCR (right). NRAV (uc001tyk.1) is indicated by red rectangle.

(B) Shown is a paradigm of the genomic location of lncRNA gene *nrav* (purple) and the relationship with gene *dynll1* (light blue). The probe for NRAV used in northern blot (NB) (red bar) and the primers for DYNLL1 (blue bar) are indicated (not scaled).

(C and D) The downregulation of NRAV in infected A549 cells was confirmed by qRT-PCR (C) (n = 3; means ± SEM; *p < 0.05) and northern blot (D). Arrow indicates the abundant form of NRAV.

(E) The 5′ and 3′ end sequences of NRAV in A549 determined by 5′ and 3′ RACE and NCBI sequences of BC065744 and BC053632 are shown.

(F) A549 cells were infected with WSN at indicated mois for 12 hr or at an moi of 3 for indicated hours. RT-PCR was performed to determine the NRAV expression.

(G) The NRAV expression in indicated human cell lines infected with/without WSN (moi = 3) for 12 hr was examined by RT-PCR. The viral nucleoprotein (NP) was examined by western blotting.

(H and I) The NRAV expression was detected in cells infected with Sendai virus (SeV), Muscovy duck reovirus (MDRV), or herpes simplex virus (HSV) by RT-PCR (H) and qRT-PCR (I).

Shown are representative RT-PCR results from three independent experiments. Data are shown as means ± SEM (n = 3; *p < 0.05; **p < 0.01). See also Figure S1 and Table S1.

altered expression of NRAV, and therefore NRAV functions unlikely through a *cis*-effect on DYNLL1 (Figures S2F and S2G). These data suggest that lncRNA NRAV is involved in regulating IAV replication, and downregulation of NRAV in infected cells might be a host self-protection response to the virus infection, which may be critical to viral clearance.

Expression of Human NRAV Significantly Increases IAV Virulence in Transgenic Mice

Although we did not succeed in detecting mouse lncRNA NRAV, mouse genome contains the *nrav* homolog sequence. To further define the role of NRAV in IAV infection, we wished to establish a more physiological model system. For this, transgenic (TG) mice expressing human NRAV were generated as previously described (Wei et al., 2014). The transgenic founders with high NRAV expression in lung were selected (Figure 3A). The TG mice and wild-type (WT) littermates were intranasally inoculated with WSN virus, and the influence of NRAV on the virulence and infection kinetics was analyzed. As expected, the IAV showed a considerably higher virulence in TG mice than that in WT mice. Under our experimental condition, body weight loss of infected TG mice was observed on day 4 postinfection (dpi) (Figure 3B). By 5–9 dpi,

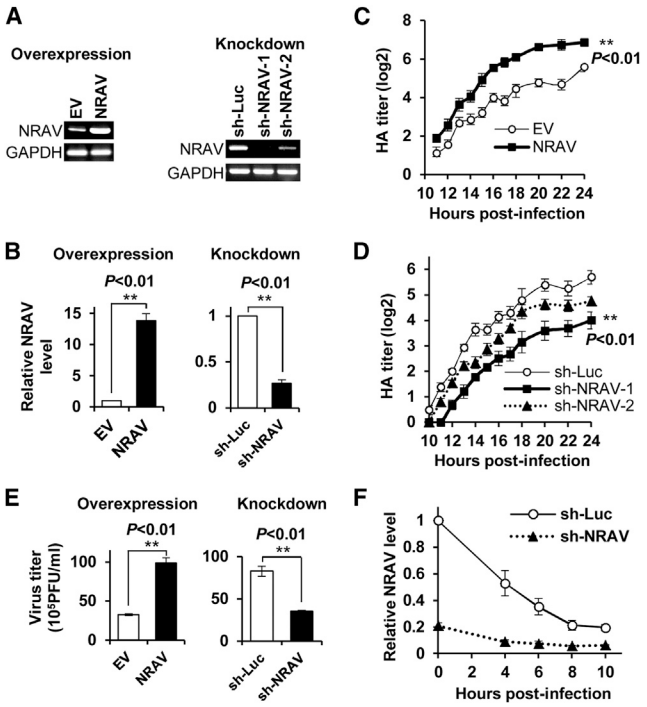

Figure 2. Altering NRAV Expression Has Profound Effects on IAV Replication in Human Cells

(A and B) The efficiency of NRAV overexpression and shRNA-based knockdown was determined by RT-PCR (A) in uninfected A549 cells or by qRT-PCR (B) in WSN infected A549 cells.

(C and D) IAV replication kinetics of NRAV-overexpressing (C) and NRAV knockdown (D) A549 cells were examined by hemagglutinin (HA) assay (moi = 0.3). The virus titers in supernatants were measured at indicated time points.

(E) IAV replication was examined by plaque assay. Virus titers in supernatants were measured at 16 hpi. Shown are representative results from infected overexpression cells (moi = 0.3) and knockdown cells (moi = 1).

(F) The expression of NRAV in infected NRAV knockdown cells was analyzed at indicated time (moi = 1) by qRT-PCR.

Cells expressing empty vector (EV) or luciferase shRNA (sh-Luc) were used as controls. n = 3; means ± SEM. See also Figure S2.

infected TG mice exhibited a consistent decrease in body weight, and with an average loss of approximately 25% on 8 dpi. All infected TG mice died within 9 dpi (Figure 3C). Under the same conditions, however, inoculated WT littermates started body weight loss on 5 dpi, with an average loss of approximately 8% on 8 dpi, and only approximately 40% of infected WT mice succumbed within 9 dpi (Figure 3C). Approximately 60% infected WT mice gained body weight gradually after 8 dpi and finally survived.

To further evaluate the in vivo effect of NRAV on IAV pathogenesis, we compared the viral loads and pathologies of the infected TG mice with WT littermates. Strikingly, the lung viral titer in TG mice was significantly higher than that in WT mice (Figure 3D), indicating more active replication of IAV in TG mice expressing NRAV. Remarkably, pathologic examination by hematoxylin and eosin (H&E) staining displayed more severe inflammation in the lungs of infected TG mice than those of the WT controls (Figure 3E). Together, these observations reveal that expression of lncRNA NRAV renders TG mice more susceptible to IAV infection.

NRAV Negatively Regulates the Expression of Several Critical ISGs

In an attempt to define the mechanism of NRAV affecting IAV replication, we performed a cDNA microarray to profile the cellular transcriptional response to NRAV overexpression in A549 cells infected with WSN for 16 hr. The microarray data displayed 882 genes upregulated and 1,538 genes downregulated (over 2-fold change, $p < 0.05$) in NRAV-overexpressing cells as compared with the controls (Figure 4A, left). Many of the differentially expressed genes were found to be associated with pathogen infection and viral reproduction through pathway analysis and Gene Ontology (GO) analysis (Figures S3A and S3B). Surprisingly, we identified 107 ISGs from differentially expressed genes in NRAV-overexpressing cells, and strikingly, the enrichment score of these ISGs was significantly high (21.3) using the analysis with interferome (Rusinova et al., 2013) (Table S2). Since ISGs are important antiviral effectors, we focused specifically on the ISG genes for further studies. Importantly, mRNA levels of some critical ISGs were significantly reduced in NRAV-overexpressing cells, including IFIT2, IFIT3, IFITM3, OASL, and MxA (Figure 4A, right). This finding was further confirmed by qRT-PCR (Figure 4B). In contrast, the mRNA levels of these ISGs were upregulated in NRAV knockdown cells (Figure 4C). Furthermore, the expression of ISGs regulated by NRAV was examined in IAV-infected NRAV TG mice and WT littermates. Consistently, we found that the levels of these ISGs in TG mice were significantly reduced as compared with those in WT controls after infection with IAV (Figures 4D and 4E). These results reveal that NRAV functions as a negative regulator of some ISGs during the IAV infection in vitro and in vivo.

Based on these data, we hypothesized that NRAV might impair host antiviral response through downregulation of some key ISGs, and if so, forced expression of these ISGs could reverse the effects of NRAV overexpression on IAV pathogenesis. To this end, exogenous IFIT2, IFIT3, IFITM3, or MxA was transiently expressed in the cell lines overexpressing NRAV or empty vector (EV) (Figure S3C). Indeed, forced expression of IFIT2, IFIT3, IFITM3, or MxA reversed the effect of NRAV on the IAV replication despite existence of excessive NRAV, whereas expression of control DDX3X, a component of TBK1-dependent innate immune response, had no such a function (Figures S3D and S3E). Because previous studies have shown that MxA interacts with IAV protein NP to inhibit the viral transcription (Mänz et al., 2013), we tested whether NRAV knockdown had any effects on IAV cRNA levels. Indeed, we found that the cRNA levels were clearly low in NRAV-depleted cells compared to the control at 8 hpi (Figure S3F), suggesting that the increased MxA caused by NRAV downregulation may block IAV transcription. However, altering NRAV expression has no significant effect on viral entry at early stage of viral infection (4 hr) (Figure S3G). These results suggest that lncRNA NRAV is critically involved in regulation of innate immune response via controlling the levels of several critical ISGs during the viral infection.

NRAV Suppresses MxA Expression Induced by Different Virus Infection and IFN Stimulation

Results presented above revealed that MxA levels were the most significantly affected by altering NRAV expression. To confirm

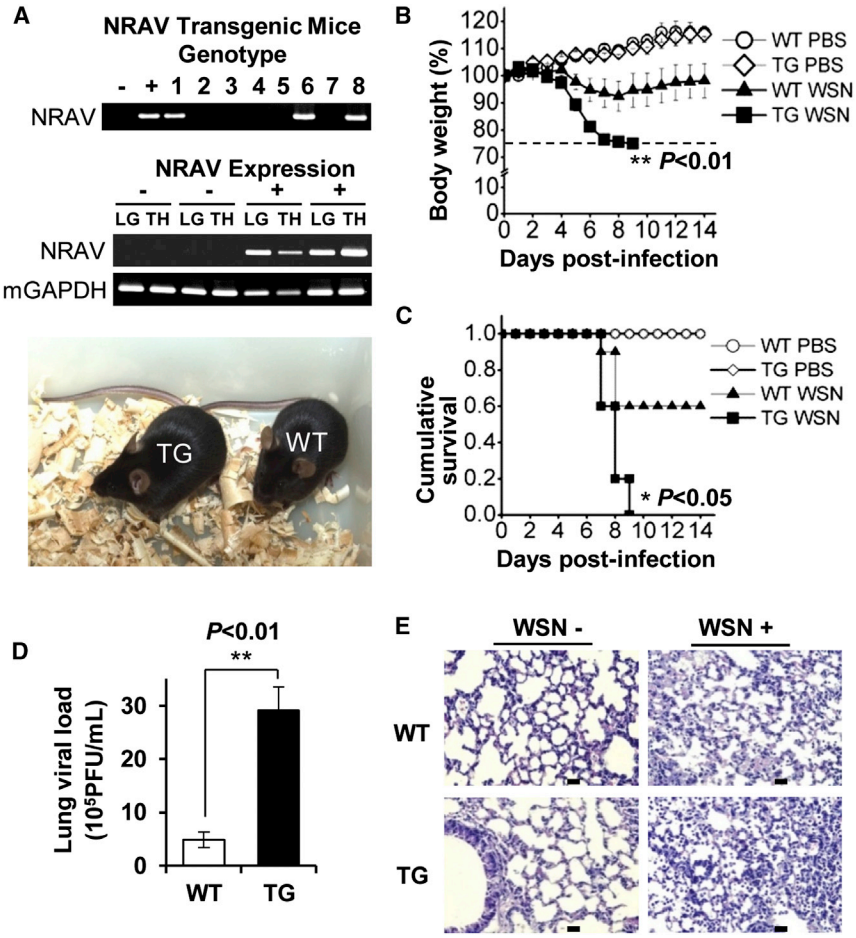

Figure 3. Expression of Human NRAV Significantly Increases IAV Virulence in Transgenic Mice

(A) The genotype (upper) and NRAV expression (middle) of C57BL/6J TG mice were determined by PCR of mouse tail DNA and RT-PCR of tissue RNA. −, WT littermates; +, TG mice; LG, lung; TH, thymus. Photo of TG and WT mice is shown (lower).

(B and C) The influence of NRAV on the WSN virulence and infection kinetics in mice were determined by body weight loss (B) and cumulative survival curve (C). Five- to six-week-old TG and WT mice were intranasally inoculated with 10^3 PFU of WSN (8–10 mice/group) or PBS (5 mice/group). The dashed line in (B) indicates the endpoint of 25% weight loss. Statistical significance in (C) was determined by log rank test.

(D) The lung viral loads in infected TG and WT mice as described in (B) were measured by plaque forming assay on day 6 (13 mice/group).

(E) Representative light photomicrographs of the mouse lung stained with HE on 6 dpi. The leukocyte infiltration was more pronounced in the infected TG mice in comparison with infected WT mice. Scale bars, 20 μm.

Data were shown as means ± SEM. *p < 0.05, **p < 0.01.

this finding, western blotting was performed to examine MxA protein. Similarly, we observed that MxA protein levels were markedly affected by altered NRAV expression (Figure S4A). Thus, MxA was selected for further studies. To further define the functional involvement of NRAV in regulating MxA expression, we investigated the effect of NRAV on MxA expression induced by different virus infections or stimulations. Interestingly, overexpression of NRAV resulted in a significant decrease in MxA expression in all cells infected with SeV for 12 hr or MDRV or HSV for 24 hr (Figures 5A–5C and S4B–S4D). In addition, when the cells were stimulated with bacterial lipopolysaccharides (LPSs) for 3 hr, the MxA level in NRAV-overexpressing cells was also significantly reduced as compared with the control cells (Figures S4E and S4F).

Because virus-induced MxA expression is regulated by cytokine-activated JAK/STAT1 signaling, we determined whether NRAV had any effects on the activation of this signaling. To test this possibility, phosphorylation of STAT1 was examined by western blotting. Surprisingly, no significant difference in the levels of p-STAT1 was observed between the infected NRAV-overexpressing cells and the control cells (Figure 5D). Our previous and current studies showed that A549 cells ectopically expressing with or without NRAV are capable of producing IFNs (Wei et al., 2014) (Figure S4G). Thus, we tested whether NRAV had effects on total cytokine levels secreted by infected cells. Consistently, no significant difference in MxA levels was detected in the fresh A549 cells stimulated with supernatants derived from either IAV-infected NRAV-overexpressing cells or infected control cells (Figures S4H and S4I, left). A similar result was obtained from the NRAV-depleted cells and the control cells (Figure S4I, right). Additionally, we found that the expression of MxA induced by IFN-β or IL29 was significantly reduced in the NRAV-overexpressing cells compared with the control (Figures 5E, 5F, S4J, and S4K). Together, these results reveal that NRAV negatively regulates MxA expression in response to broad stimulations without significantly altering total cytokine production and JAK/STAT1 signaling.

NRAV Inhibits the Initial Transcription of MxA and IFITM3, Likely through Regulating Histone Modifications of the ISG Genes

Next, we investigated how NRAV might regulate the ISG expression. To this end, we determined the cellular localization of NRAV and found that although NRAV was localized both in the cytoplasm and nucleus, more NRAV was distributed in the nucleus of A549 cell (Figures 6A and S5A). Thus, we presumed that NRAV might be involved in transcriptional control of these ISGs. The pre-mRNA level can represent the initial transcription rate. Therefore, the primers to examine the pre-mRNA levels of MxA (preMxA) and IFITM3 (preIFITM3) were designed as previously described (Zeisel et al., 2011) (Figure 6B). We observed that the preMxA and preIFITM3 levels in infected NRAV-overexpressing cells were lower than those in control ($p < 0.05$), while no bands were observed in no reverse transcriptase control

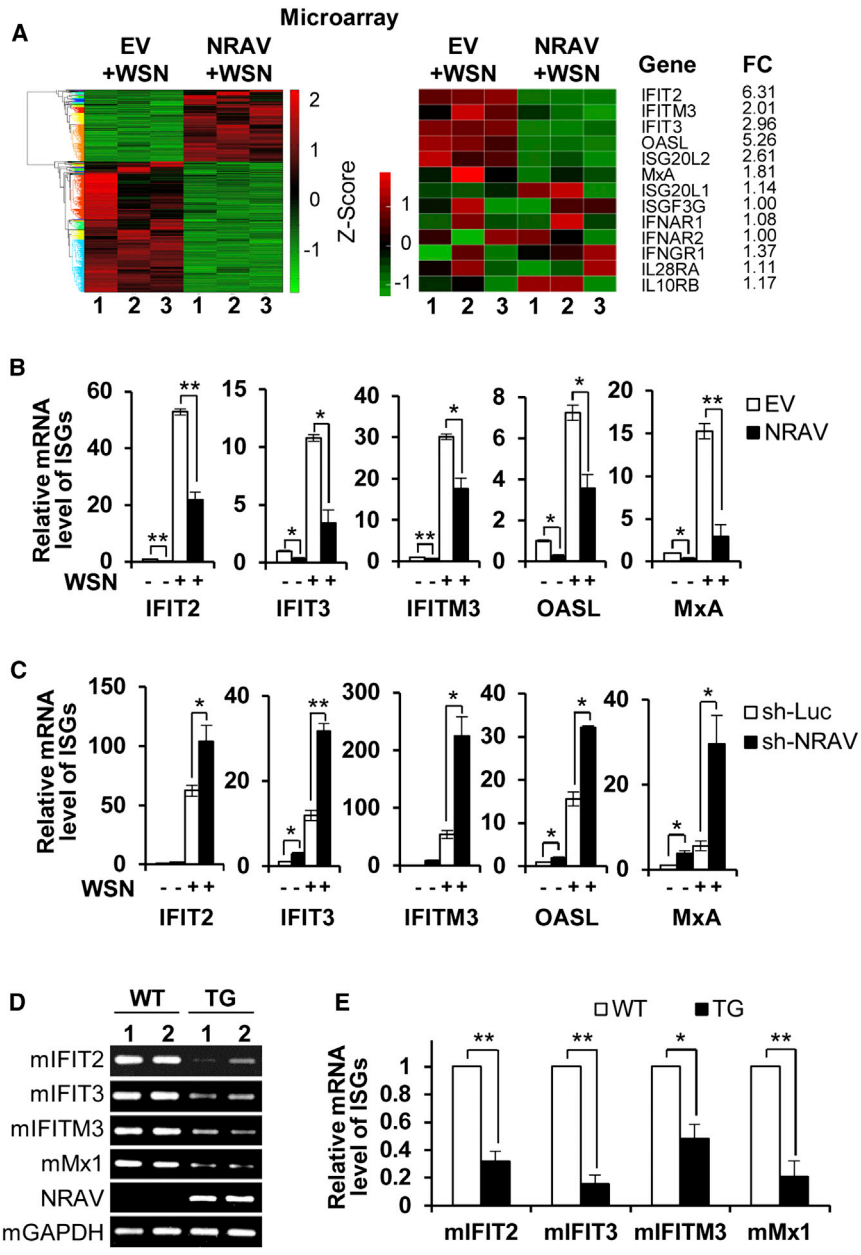

Figure 4. NRAV Negatively Regulates the Expression of Several Critical ISGs

(A) cDNA microarray analysis displayed hundreds of genes differentially expressed (n = 3, fold change > 2.0, $p < 0.05$) in WSN infected NRAV-overexpressing cells compared with control (moi = 3; 16 hpi) (left). Significantly changed ISGs and unchanged ISGs and IFN receptors are shown (right). The RNA quantitation data are shown as centered and scaled log2 data in heatmaps.

(B and C) The mRNA levels of ISGs in NRAV-expressing and EV control cells (B) or NRAV knockdown and sh-Luc control cells (C) infected with or without WSN were determined by qRT-PCR (n = 3).

(D and E) The mRNA levels of mIFIT2, mIFIT3, mIFITM3, and mMx1 in infected TG or WT mouse lungs were determined by RT-PCR (D) or by qRT-PCR (E). In (D), 1 and 2 indicate two individuals. Data are shown as means ± SEM. *$p < 0.05$, **$p < 0.01$. See also Figure S3 and Table S2.

(Figures 6C–6E), indicating that NRAV may regulate the initial transcription of MxA and IFITM3. Furthermore, we observed that the promoter activity of both MxA and IFITM3 was significantly reduced in NRAV-overexpressing cells compared with control cells using a luciferase reporter assay (Figures S5B–S5D). These observations suggest that NRAV may be involved in negative regulation of promoter function of these ISGs.

Because lncRNAs were shown to silence gene transcription through maintenance of DNA methylation (Mohammad et al., 2012) and *mxA* contains a low CpG promoter (Ramirez-Carrozzi et al., 2009), we determined whether NRAV affected the DNA methylation of *mxA* gene. As shown in Figure S5E, treatment of A549 cells with DNA methyltransferase inhibitor decitabine (DAC) resulted in an increase of MxA mRNA level. However, expression of MxA was still inhibited in the presence of NRAV. In addition, we examined the mRNA decay rate of MxA in the infected cells treated with actinomycin D (ActD), since lncRNAs can activate mRNA decay through recruiting STAU1 to mRNAs (Kretz et al., 2013). No significant difference in the mRNA degradation rates was detected between NRAV-overexpressing cells and control cells (Figures S5F and S5G). These data indicate that NRAV may be not associated with MxA DNA methylation and post-transcriptional regulation of MxA.

Histone modification at transcription start sites is a crucial step for the regulation of gene transcription, and previous studies have proposed that lncRNAs are involved in these processes (Wang and Chang, 2011). Next, we investigated the histone 3 lysine 4 trimethylation (H3K4me3) as an active mark and histone 3 lysine 27 trimethylation (H3K27me3) as a repression signal by performing chromatin immunoprecipitation (ChIP). We found that the H3K4me3 enrichments at the *mxA* and *ifitm3* transcription start sites in NRAV-overexpressing cells were obviously impaired as compared with those in control cells following IAV infection (Figures 6F and S5H). In contrast, the H3K27me3 enrichment at *mxA* gene locus in infected NRAV-overexpressing cells exhibited remarkably higher than that in control cells, although the H3K27me3 enrichment at *ifitm3* remained unchanged (Figures 6G and S5I). Consistently, NRAV knockdown resulted in a significant increase in H3K4me3 enrichments and a significant decrease in H3K27me3 enrichments at *mxA* and *ifitm3* transcription start sites (Figures S5J and S5K). These data reveal that NRAV may function to inhibit the ISG transcription by affecting the histone modifications of these genes.

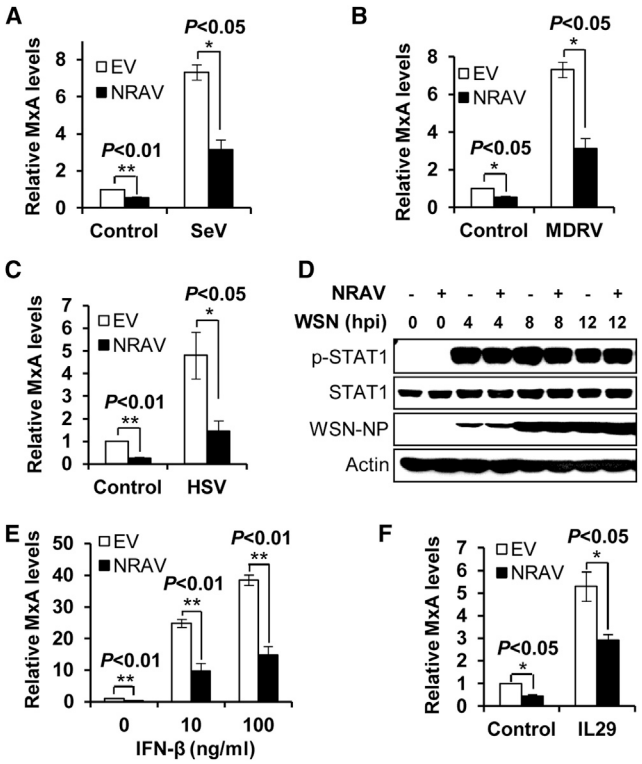

Figure 5. NRAV Suppresses MxA Expression Induced by Different Virus Infection and IFN Stimulation

(A–C) The MxA mRNA levels in following NRAV cells and EV cells were determined by qRT-PCR: SeV infected A549 cells (A), MDRV infected 293T cells (B), and HSV infected A549 cells (C) (means ± SEM; n = 3).

(D) A549 cells overexpressing NRAV or control were infected with WSN for indicated time. STAT1 and its Tyr701-phosphorylation were determined by western blotting.

(E and F) The MxA mRNA levels in NRAV overexpressing cells and control A549 cells stimulated by IFN-β (E) or IL29 (F) (50 ng/ml) for 3 hr were detected by qRT-PCR (means ± SEM; n = 3). *p < 0.05, **p < 0.01. See also Figure S4.

To further identify the functional protein partners of NRAV, we performed RNA pull-down by using biotinylated NRAV antisense probes or scramble control probes. Interestingly, a specific NRAV-bound protein in resting A549 cells was pulled down and identified to be ZO-1-associated nucleic acid binding protein (ZONAB) by mass spectrometry (Figures 6H and S6A; Table S3). This finding was further confirmed by RNA immunoprecipitation (RIP) showing that the amount of NRAV precipitated with anti-ZONAB Ab was dramatically higher than that of GAPDH control (Figure S6B). We next determined the role of ZONAB in MxA expression. The shRNA-based ZONAB knockdown was performed and verified by qRT-PCR (Figure S6C). Interestingly, the levels of MxA mRNA were significantly decreased after silencing ZONAB in both infected and uninfected cells (Figure 6I). When ZONAB was depleted in NRAV-overexpressing cells, the MxA mRNA was decreased to a lower level (Figure 6J), while NRAV was not affected by altered ZONAB expression (Figure S6D, left). Consistently, the exogenous expression of ZONAB in NRAV-overexpressing cells partially reversed the NRAV-mediated suppression of MxA expression (Figures S6D–S6F). These results indicate that ZONAB is involved in MxA transcription as a positive regulator.

The Spatial Structure of Functional Moieties Was Essential for lncRNA NRAV Function

The diverse functions of lncRNAs are based on their propensity to fold into thermodynamically stable secondary and higher-order structures (Mercer and Mattick, 2013). To determine the functional structures of lncRNA NRAV, we designed and constructed eight truncation and deletion mutants based on the predicted secondary structure of NRAV through three softwares, RNAfold (Gruber et al., 2008), Centroidfold, and Genebee (Figures 7A and 7B). As displayed, mutant A (mutA) lacks the stem-loop arm A, while contains other stem-loop structures or elements (arms C, D, and E) as compared with the intact NRAV (Figure 7A). Ectopic expression of these mutants was determined by RT-PCR (Figure 7B, right). Interestingly, experiments testing the effects of these mutants on virus replication demonstrated that all examined structure moieties of NRAV except arm D, which was a small arm of NRAV (nt 618–872), were required for its role in controlling IAV replication (Figure 7C). Consistently, the reduction of MxA mRNA level was detected only in cells ectopically expressing WT NRAV or its mutD (Figure 7D). These experiments demonstrate that RNA sequences of stem loops in NRAV except nt 618–872 may form a spatial structure that is essential for its function.

DISCUSSION

Although much emphasis has been placed on investigating host protein factors in the activation of innate immune responses to IAV infection, little is known about the role of lncRNAs in these processes. lncRNA THRIL, NeST, NEAT, and lincRNA-Cox2 have been reported to regulate the expression of TNF-α, IFN-γ, IL8, and inflammatory response, respectively (Carpenter et al., 2013; Gomez et al., 2013; Imamura et al., 2014; Li et al., 2014). Here we report a human lncRNA named as NRAV, which is expressed in various human cells, but significantly downregulated during the IAV infection and infections with ssRNA virus (SeV), dsRNA virus (MDRV), and DNA virus (HSV). Importantly, we have revealed that overexpression of NRAV promotes the IAV replication in vitro and in vivo by suppressing the expression of several key ISGs, such as IFIT2, IFIT3, IFITM3, and MxA, very likely through affecting the histone modifications of these ISG genes. These findings establish that NRAV functions as an important regulatory molecule via negatively regulating the expression of some crucial antiviral proteins, which modulates the host innate immune response against IAV infection and maybe more broadly involved in other viral infections.

In uninfected cells, NRAV likely contributes to precise control of the expression of these critical ISGs. When virus infection is sensed, the reduction of NRAV would benefit the rapid accumulation of the antiviral proteins to facilitate the clearance of virus. Therefore, downregulation of NRAV may be initiated by host as a self-protection response. This is coherent with the tight and exquisite control of antiviral response that ensures rapid defense against pathogens with minimal inflammatory damage. A number of negative regulators of innate immunity have been found, such as SOCS1 and SOCS3, which negatively regulate

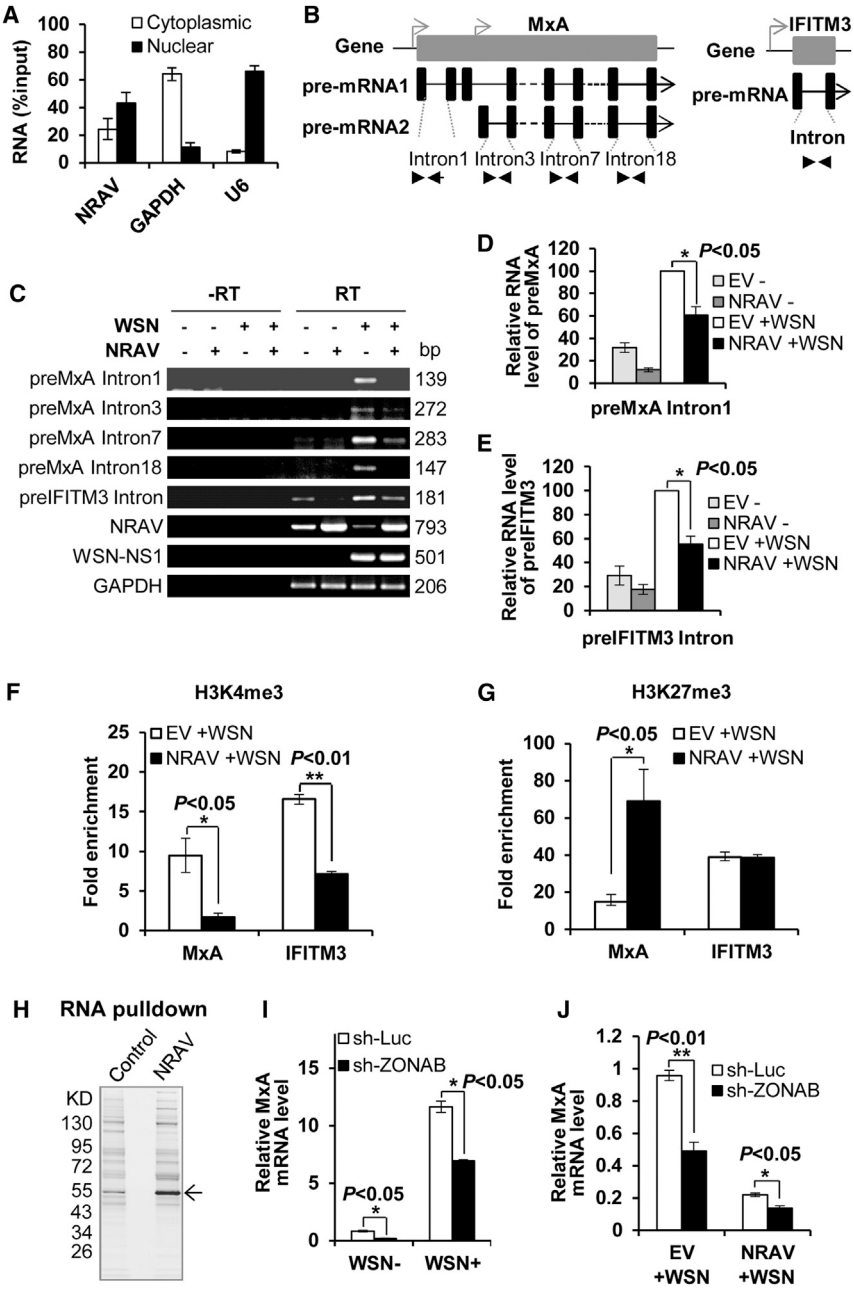

Figure 6. NRAV Inhibits the Initial Transcription of MxA and IFITM3 through Regulating Histone Modifications of the ISG Genes

(A) The RNA levels of NRAV, cytoplasmic control (GAPDH mRNA), and nuclear control (U6 RNA) were assessed by qRT-PCR in cytoplasmic and nuclear fractions from A549. The total RNA was used as input control. Data are shown as % input (means ± SEM; n = 3.)

(B) Paradigms of the pre-mRNA sturctures of MxA (left) and IFITM3 (right) (not scaled). Introns (black line) between two exons (black block) used for pre-mRNA detection are indicated. Several pairs of primers were used to detect two isoforms of pre-MxA. Corresponding primers are shown as a pair of arrows. Promoters are shown as bended arrows.

(C–E) The pre-mRNA levels of MxA (preMxA) and IFITM3 (preIFITM3) in IAV infected NRAV-overexpressing cells or EV control cells were determined by RT-PCR (C) and qRT-PCR (preMxA [D], preIFITM3 [E]). Shown are representative data of three independent experiments. Means ± SEM; n = 3. *p < 0.05. −RT, no reverse transcriptase in reverse transcription (RT). RT, normal reaction. The length of RT-PCR product is shown.

(F and G) ChIP analysis of H3K4me3 (F) and H3K27me3 (G) levels at the *mxA* and *ifitm3* locus in IAV-infected NRAV-overexpressing or control cells. The relative amounts of *mxA* and *ifitm3* DNA immunoprecipitated by the anti-H3K4me3 or anti-H3K27me3 antibody were normalized to that isolated by the control IgG. The fold enrichment was calculated as $2^{-\Delta\Delta Ct}$ (mean ± SEM; n = 3).

(H) Silver staining of proteins pulled down by NRAV antisense probes or scramble control probes from A549 cell lysate. The specific NRAV-associated band (arrow) was excised for mass spectrometry. Shown are representative data from three independent experiments.

(I) MxA mRNA levels in ZONAB-depleted A549 cells infected with or without WSN (moi = 1, 12 hpi) were measured by qRT-PCR and normalized to that of uninfected control cells transfected with vector sh-Luc.

(J) Experiments were performed as described in (I). MxA mRNA levels in ZONAB-depleted NRAV-overexpressing A549 cells were measured by qRT-PCR.

Data are shown as means ± SEM; n = 3. *p < 0.05, **p < 0.01. See also Figures S5–S7 and Table S3.

IFN-activated JAK-STAT signaling to control the ISG transcriptional response to IFN stimulation (Akhtar and Benveniste, 2011). LincRNA-Cox2 also mediates the repression of some immune genes (Carpenter et al., 2013). Although the mechanism underlying downregulation of NRAV by viral infection remains elusive, the expression of NRAV is likely controlled by particular pathways activated upon sensing the viral infection. Indeed, we found that the NRAV downregulation was induced only by viral RNA which is produced during virus replication (Figures S7A–S7E) and newly synthesized protein(s) (Figure S7F). However, these proteins might include neither virus-induced cytokines nor IFNAR1 (Figures S7G–S7J). We observed that reduction of NRAV was not caused by increase in RNA decay (Figure S7K), indicating that this protein(s) might be relevent with the transcriptional regulation of NRAV. CpG islands and some transcription factor binding sites on the upstream of *nrav* were predicted (Figure S7L). Interestingly, DNA methyltransferase might participate in the regulation of NRAV (Figures S7M–S7P). These findings suggest that virus infection might induce the transcription inhibition of *nrav* through epigenetic modification.

We identified that NRAV critically regulated several key antiviral effectors in innate immunity. Strikingly, the transcriptional regulations of these genes are distinct, and multiple mechanisms are involved. For example, MxA/Mx1 is regulated through strictly IFN-dependent pathway, while IFIT2 and IFIT3 are through both IFN-dependent and IFN-independent pathways

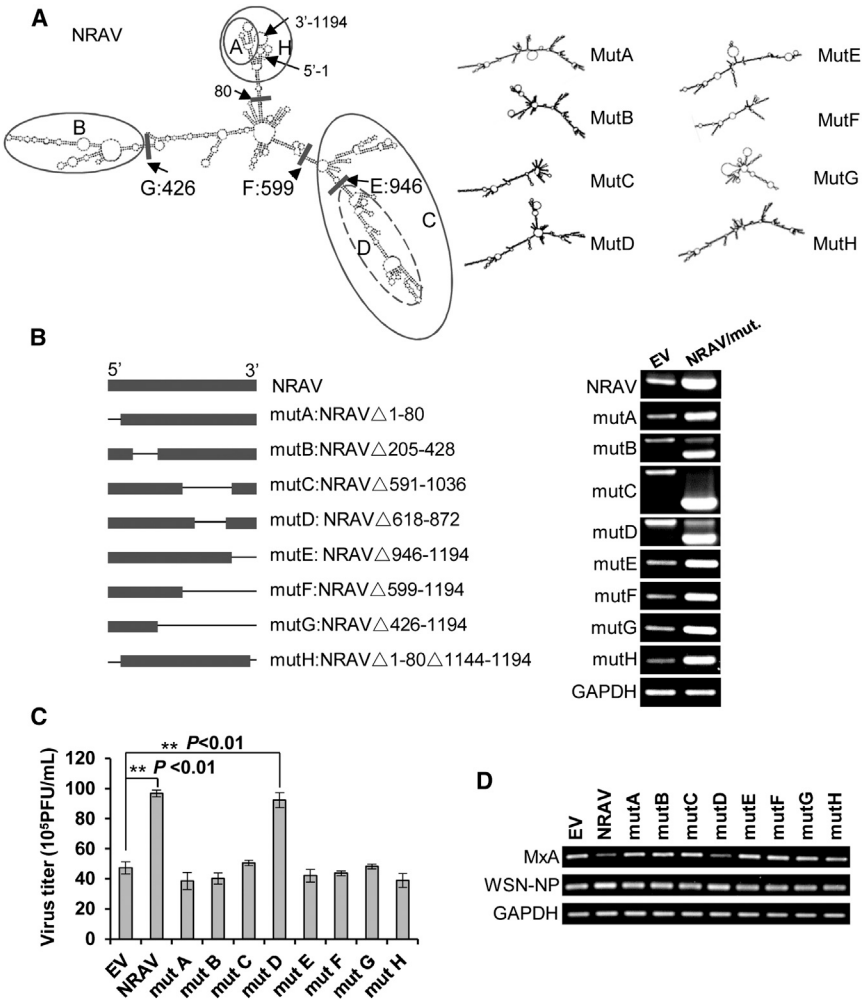

Figure 7. The Spatial Structure of Functional Moieties Was Essential for lncRNA NRAV Activity

(A) Secondary structure predictions of NRAV and mutations were performed through three softwares (RNAfold, Certroidfold, and Genebee). The mutation locations were labeled by circle or short bar.

(B) Schematic diagram of truncation and deletion mutations of NRAV is shown (left). The stable exogenous expression of NRAV or its mutants in A549 cells was determined by RT-PCR (right).

(C) A549 cells expressing NRAV or its mutants were infected with IAV, and the virus titers in culture supernatants were determined through plaque-forming assay (n = 3; means ± SEM; $^{**}p < 0.01$).

(D) The MxA mRNA levels in A549 cells in (C) were detected by RT-PCR. Shown are representative results from three independent experiments.

(Lazear et al., 2013). Interestingly, these NRAV-modulated ISGs have recently been reported belonging to a subset of ISGs which are regulated by an IKKi-associated specific signal pathway (Ng et al., 2011; Tenoever et al., 2007). In this study, we found that the initial transcription rates of MxA and IFITM3 were reduced and the histone modifications (active mark H3K4me3 and repressive mark H3K27me3) were altered by NRAV. Several lncRNAs have been reported to regulate chromatin remodeling on specific gene location through directly binding with hnRNPs (Carpenter et al., 2013; Li et al., 2014). Although we have excluded the possibility that NRAV functions through regulating IFN-JAK/STAT1 pathway, the molecular mechanism by which NRAV regulates the initial transcription and histone modifications remains unknown. On the other hand, NRAV was shown to interfere with the MxA and IFITM3 promoter activity in a luciferase reporter system. These data suggest that there might exist multiple mechanisms underlying NRAV-mediated regulation of ISG transcription.

It has been thought that lncRNAs usually interact with other molecules to exert regulatory activities. In this study, ZONAB was identified as a NRAV-associated protein involved in MxA transcription regulation. ZONAB is a multifunctional protein that regulates transcription of cyclin D1 and PCNA as an important transcription factor and posttranscriptionally regulates other protein and mRNA levels in cytoplasm (Lima et al., 2010; Nie et al., 2012). Although it is unclear whether ZONAB functions as a transcription factor of ISG expression, we found a ZONAB binding sequence (invert CCAAT) at −219 to −215 of MxA transcription start region (Dolfini and Mantovani, 2013), suggesting the potential involvement of ZONAB in initial transcription of MxA. Additionally, as a transcription factor ZONAB might also be involved in histone modifications and nucleosome packing (Rothenberg, 2014). It has been thought that ZONAB can upregulate several chromatin remodeling components (histone H4 and HMG-I) and MYC that recruits core histone-modifying enzymes to DNA (Sourisseau et al., 2006). Further experiments are needed in the future to address how ZONAB interacts with NRAV to regulate ISG expression.

Human NRAV is an intronic antisense lncRNA of dynein light-chain gene *dynll1*. Although Dynein is shown to be recruited by many viruses to facilitate their replication and enhance their spread, and direct interaction of Dynll with virions is identified (Merino-Gracia et al., 2011), we did not observe significant change in the Dynll1 levels after altering the NRAV expression (GEO accession number GSE48874; Figures S2F and S2G). Of interest is that hundreds of genes differentially expressed in NRAV-overexpressing cells and the pathway and GO analysis indicated that many are associated with pathogen infection and viral reproduction. In addition, the expression of NRAV in different types of human cells also indicates its broad functions. The expression of human NRAV in multiple tissues of TG mice including lung, thymus, and bone marrow might be important for the IAV pathogenesis. Therefore, the role of NRAV may be not limited to the modulation of ISGs. Moreover, the decline of

NRAV level can also be induced by other RNA/DNA virus infections. Hence, we surmise that NRAV-related cellular response may be a universal defense against virus infection. The exact relationship between NRAV distribution in different tissues and its antiviral activities needs to be determined.

EXPERIMENTAL PROCEDURES

Microarray and Data Analysis

The lncRNA cDNA microarray was from Arraystar (Arraystar, Rockville, MD). The cDNA microarray was performed using Human 12x135K gene expression microarray (Roche NimbleGen, Madison, WI). Total RNAs from three independent groups of WSN-infected A549 cells or control cells were prepared using Trizol reagent (Invitrogen, Carlsbad, CA). cDNA synthesis, labeling, hybridization, and data analysis were carried out as previously described (Guo et al., 2014) (see Supplemental Information).

Cells, Viruses, Antibodies, and Plasmids

Cells, viruses, and antibodies were described in the Supplemental Information. For plasmid construction, human IFIT2, IFIT3, IFITM3, MxA, and DDX3X were subcloned into the pcDNA3.1 and pCMV5a vectors. shRNA-based knockdown plasmids were generated with a pSIH-H1-GFP lentiviral vector expressing shRNA.

Viral Infection and Virus Titers Assay

A549 cells were infected with IAV WSN, Sendai virus (SeV), or herpes simplex virus (HSV), and 293T cells were infected with Muscovy duck reovirus (MDRV). Virus titers in supernatants were determined (see Supplemental Information).

5′ and 3′ RACE

The 5′ and 3′ RACE analyses were performed using the SMARTer RACE cDNA amplification Kit (Clontech) as per the manufacturer's instructions. RACE PCR products were cloned into pZeroBack (Tiangen, Beijing, China) and sequenced.

Transgenic Mice and Virus Challenge

The mouse experimental design and protocols used in this study were approved by the Research Ethics Committee of Institute of Microbiology, Chinese Academy of Sciences (permit number PZIMCAS2012001). The studies of mice were performed in strict accordance with the Regulation of Institutional Research Ethics Committee of Institute of Microbiology. The NRAV transgenic C57BL/6 mice were created as previously described (Wang et al., 2014; Wei et al., 2014). Mice were inoculated intranasally with WSN. Mouse lungs were collected for lung viral loads assay and H&E staining (see Supplemental Information).

RNA Pull-Down Assay, RNA Immunoprecipitation, and Chromatin Immunoprecipitation

Uninfected A549 cell lysates were used for RNA pull-down assay and RIP, and IAV-infected A549 cells were subjected to ChIP assays using the Magna ChIP A/G chromatin immunoprecipitation kit (Millipore) following the manufacturer's instruction as described in Supplemental Information.

Generation of Stable Cell Lines and Cell Stimulation

The stable NRAV-overexpressing cells and A549 cell lines stably expressing specific ISGs were generated with a retroviral expression system by infecting the cells with retroviruses encoding these genes. Recombinant human IFN-β and IL29 were purchased from PeproTech (Rocky Hill, NJ). For stimulation, unless indicated, cells were incubated for 2–3 hr with the recombinant cytokines or peptides (see Supplemental Information).

Western Blotting and Northern Blotting

For western blotting, cell lysates were separated by SDS-polyacrylamide gel electrophoresis, transferred onto a nitrocellulose membrane, and probed with indicated antibodies as described previously (Wei et al., 2014). For northern blotting, total RNA of A549 cell was isolated using Trizol reagent. Probe is a DNA fragment of NRAV (793 bp, 358–1,150), which was radiolabeled by using Prime-a-Gene Labeling System (Promega). The assay was performed by using Northernmax-gly kit (Invitrogen) and autoradiography.

Statistical Analysis

Comparison between groups was made using Student's t test. Data represent the mean ± SEM. Differences were considered statistically significant with $p < 0.05$.

ACCESSION NUMBERS

The GenBank accession number for the *nrav* gene sequence reported in this paper is KF311770. The Gene Expression Omnibus accession numbers for the microarray data reported in this paper are GSE32878 and GSE48874.

SUPPLEMENTAL INFORMATION

Supplemental Information includes seven figures, three tables, and Supplemental Experimental Procedures and can be found with this article at http://dx.doi.org/10.1016/j.chom.2014.10.001.

AUTHOR CONTRIBUTIONS

J.O. and J.-L.C. designed research; J.O., X.Z., Y.C., H.W., Q.C., X.C., and B.Q. performed experiments; L.Z. and Y.Z. contributed new reagents and analytic tools; J.O., G.F.G., G.W., and J.-L.C. analyzed data; J.O. and J.-L.C. wrote the manuscript.

ACKNOWLEDGMENTS

We thank Drs. Guijie Guo and Jun Wu and members of Runsheng Chen's lab for assistance with ChIP and RIP experiments and for bioinformatics analysis. This work was supported by National Key Technologies Research and Development Program of China (2013ZX10004-611), National Basic Research Program (973) of China (2015CB910502), Natural Science Foundation of China (U1305212), and Intramural grant of the Chinese Academy of Sciences (KJZD-EW-L01-3) to J.-L.C., and by a grant from China Postdoctoral Science Foundation (2012M510585) to J.O.

Received: March 2, 2014
Revised: June 4, 2014
Accepted: September 15, 2014
Published: November 12, 2014

REFERENCES

Akhtar, L.N., and Benveniste, E.N. (2011). Viral exploitation of host SOCS protein functions. J. Virol. *85*, 1912–1921.

Carpenter, S., Aiello, D., Atianand, M.K., Ricci, E.P., Gandhi, P., Hall, L.L., Byron, M., Monks, B., Henry-Bezy, M., Lawrence, J.B., et al. (2013). A long noncoding RNA mediates both activation and repression of immune response genes. Science *341*, 789–792.

Cullen, B.R. (2013). Making a NeST for a persistent virus. Cell Host Microbe *13*, 241–242.

Dolfini, D., and Mantovani, R. (2013). Targeting the Y/CCAAT box in cancer: YB-1 (YBX1) or NF-Y? Cell Death Differ. *20*, 676–685.

Everitt, A.R., Clare, S., Pertel, T., John, S.P., Wash, R.S., Smith, S.E., Chin, C.R., Feeley, E.M., Sims, J.S., Adams, D.J., et al.; GenISIS Investigators; MOSAIC Investigators (2012). IFITM3 restricts the morbidity and mortality associated with influenza. Nature *484*, 519–523.

Fensterl, V., Wetzel, J.L., Ramachandran, S., Ogino, T., Stohlman, S.A., Bergmann, C.C., Diamond, M.S., Virgin, H.W., and Sen, G.C. (2012). Interferon-induced Ifit2/ISG54 protects mice from lethal VSV neuropathogenesis. PLoS Pathog. *8*, e1002712.

Gomez, J.A., Wapinski, O.L., Yang, Y.W., Bureau, J.F., Gopinath, S., Monack, D.M., Chang, H.Y., Brahic, M., and Kirkegaard, K. (2013). The NeST long

ncRNA controls microbial susceptibility and epigenetic activation of the interferon-γ locus. Cell *152*, 743–754.

Gruber, A.R., Lorenz, R., Bernhart, S.H., Neuböck, R., and Hofacker, I.L. (2008). The Vienna RNA websuite. Nucleic Acids Res. *36* (Web Server issue), W70–W74.

Guo, G., Kang, Q., Zhu, X., Chen, Q., Wang, X., Chen, Y., Ouyang, J., Zhang, L., Tan, H., Chen, R., et al. (2014). A long noncoding RNA critically regulates Bcr-Abl-mediated cellular transformation by acting as a competitive endogenous RNA. Oncogene. http://dx.doi.org/10.1038/onc.2014.131.

Guttman, M., and Rinn, J.L. (2012). Modular regulatory principles of large noncoding RNAs. Nature *482*, 339–346.

Imamura, K., Imamachi, N., Akizuki, G., Kumakura, M., Kawaguchi, A., Nagata, K., Kato, A., Kawaguchi, Y., Sato, H., Yoneda, M., et al. (2014). Long noncoding RNA NEAT1-dependent SFPQ relocation from promoter region to paraspeckle mediates IL8 expression upon immune stimuli. Mol. Cell *53*, 393–406.

Kretz, M., Siprashvili, Z., Chu, C., Webster, D.E., Zehnder, A., Qu, K., Lee, C.S., Flockhart, R.J., Groff, A.F., Chow, J., et al. (2013). Control of somatic tissue differentiation by the long non-coding RNA TINCR. Nature *493*, 231–235.

Lazear, H.M., Lancaster, A., Wilkins, C., Suthar, M.S., Huang, A., Vick, S.C., Clepper, L., Thackray, L., Brassil, M.M., Virgin, H.W., et al. (2013). IRF-3, IRF-5, and IRF-7 coordinately regulate the type I IFN response in myeloid dendritic cells downstream of MAVS signaling. PLoS Pathog. *9*, e1003118.

Li, Z., Chao, T.C., Chang, K.Y., Lin, N., Patil, V.S., Shimizu, C., Head, S.R., Burns, J.C., and Rana, T.M. (2014). The long noncoding RNA THRIL regulates TNFα expression through its interaction with hnRNPL. Proc. Natl. Acad. Sci. USA *111*, 1002–1007.

Lima, W.R., Parreira, K.S., Devuyst, O., Caplanusi, A., N'kuli, F., Marien, B., Van Der Smissen, P., Alves, P.M., Verroust, P., Christensen, E.I., et al. (2010). ZONAB promotes proliferation and represses differentiation of proximal tubule epithelial cells. J. Am. Soc. Nephrol. *21*, 478–488.

Lin, M.F., Jungreis, I., and Kellis, M. (2011). PhyloCSF: a comparative genomics method to distinguish protein coding and non-coding regions. Bioinformatics *27*, i275–i282.

Liu, X.Y., Chen, W., Wei, B., Shan, Y.F., and Wang, C. (2011). IFN-induced TPR protein IFIT3 potentiates antiviral signaling by bridging MAVS and TBK1. J. Immunol. *187*, 2559–2568.

Mänz, B., Dornfeld, D., Götz, V., Zell, R., Zimmermann, P., Haller, O., Kochs, G., and Schwemmle, M. (2013). Pandemic influenza A viruses escape from restriction by human MxA through adaptive mutations in the nucleoprotein. PLoS Pathog. *9*, e1003279.

Mercer, T.R., and Mattick, J.S. (2013). Structure and function of long noncoding RNAs in epigenetic regulation. Nat. Struct. Mol. Biol. *20*, 300–307.

Mercer, T.R., Dinger, M.E., and Mattick, J.S. (2009). Long non-coding RNAs: insights into functions. Nat. Rev. Genet. *10*, 155–159.

Merino-Gracia, J., García-Mayoral, M.F., and Rodríguez-Crespo, I. (2011). The association of viral proteins with host cell dynein components during virus infection. FEBS J. *278*, 2997–3011.

Mohammad, F., Pandey, G.K., Mondal, T., Enroth, S., Redrup, L., Gyllensten, U., and Kanduri, C. (2012). Long noncoding RNA-mediated maintenance of DNA methylation and transcriptional gene silencing. Development *139*, 2792–2803.

Ng, S.L., Friedman, B.A., Schmid, S., Gertz, J., Myers, R.M., Tenoever, B.R., and Maniatis, T. (2011). IκB kinase epsilon (IKK(epsilon)) regulates the balance between type I and type II interferon responses. Proc. Natl. Acad. Sci. USA *108*, 21170–21175.

Nie, M., Balda, M.S., and Matter, K. (2012). Stress- and Rho-activated ZO-1-associated nucleic acid binding protein binding to p21 mRNA mediates stabilization, translation, and cell survival. Proc. Natl. Acad. Sci. USA *109*, 10897–10902.

Peng, X., Gralinski, L., Armour, C.D., Ferris, M.T., Thomas, M.J., Proll, S., Bradel-Tretheway, B.G., Korth, M.J., Castle, J.C., Biery, M.C., et al. (2010). Unique signatures of long noncoding RNA expression in response to virus infection and altered innate immune signaling. mBio. *1*, e00206–e00210.

Ramirez-Carrozzi, V.R., Braas, D., Bhatt, D.M., Cheng, C.S., Hong, C., Doty, K.R., Black, J.C., Hoffmann, A., Carey, M., and Smale, S.T. (2009). A unifying model for the selective regulation of inducible transcription by CpG islands and nucleosome remodeling. Cell *138*, 114–128.

Rothenberg, E.V. (2014). The chromatin landscape and transcription factors in T cell programming. Trends Immunol. *35*, 195–204.

Rusinova, I., Forster, S., Yu, S., Kannan, A., Masse, M., Cumming, H., Chapman, R., and Hertzog, P.J. (2013). Interferome v2.0: an updated database of annotated interferon-regulated genes. Nucleic Acids Res. *41* (Database issue), D1040–D1046.

Smale, S.T. (2012). Transcriptional regulation in the innate immune system. Curr. Opin. Immunol. *24*, 51–57.

Sourisseau, T., Georgiadis, A., Tsapara, A., Ali, R.R., Pestell, R., Matter, K., and Balda, M.S. (2006). Regulation of PCNA and cyclin D1 expression and epithelial morphogenesis by the ZO-1-regulated transcription factor ZONAB/DbpA. Mol. Cell. Biol. *26*, 2387–2398.

Tenoever, B.R., Ng, S.L., Chua, M.A., McWhirter, S.M., García-Sastre, A., and Maniatis, T. (2007). Multiple functions of the IKK-related kinase IKKepsilon in interferon-mediated antiviral immunity. Science *315*, 1274–1278.

Wang, K.C., and Chang, H.Y. (2011). Molecular mechanisms of long noncoding RNAs. Mol. Cell *43*, 904–914.

Wang, T., Tian, C., Zhang, W., Luo, K., Sarkis, P.T., Yu, L., Liu, B., Yu, Y., and Yu, X.F. (2007). 7SL RNA mediates virion packaging of the antiviral cytidine deaminase APOBEC3G. J. Virol. *81*, 13112–13124.

Wang, S., Chi, X., Wei, H., Chen, Y., Chen, Z., Huang, S., and Chen, J.L. (2014). Influenza A virus-induced degradation of eukaryotic translation initiation factor 4B contributes to viral replication by suppressing IFITM3 protein expression. J. Virol. *88*, 8375–8385.

Wei, H., Wang, S., Chen, Q., Chen, Y., Chi, X., Zhang, L., Huang, S., Gao, G.F., and Chen, J.L. (2014). Suppression of interferon lambda signaling by SOCS-1 results in their excessive production during influenza virus infection. PLoS Pathog. *10*, e1003845.

Winterling, C., Koch, M., Koeppel, M., Garcia-Alcalde, F., Karlas, A., and Meyer, T.F. (2014). Evidence for a crucial role of a host non-coding RNA in influenza A virus replication. RNA Biol. *11*, 66–75.

Yin, Z., Guan, D., Fan, Q., Su, J., Zheng, W., Ma, W., and Ke, C. (2013). lncRNA expression signatures in response to enterovirus 71 infection. Biochem. Biophys. Res. Commun. *430*, 629–633.

Zeisel, A., Köstler, W.J., Molotski, N., Tsai, J.M., Krauthgamer, R., Jacob-Hirsch, J., Rechavi, G., Soen, Y., Jung, S., Yarden, Y., and Domany, E. (2011). Coupled pre-mRNA and mRNA dynamics unveil operational strategies underlying transcriptional responses to stimuli. Mol. Syst. Biol. *7*, 529.

Zhang, Q., Chen, C.Y., Yedavalli, V.S., and Jeang, K.T. (2013). NEAT1 long noncoding RNA and paraspeckle bodies modulate HIV-1 posttranscriptional expression. mBio. *4*, e00596–e00512.

Cell Host & Microbe, Volume *16*

Supplemental Information

NRAV, a Long Noncoding RNA, Modulates Antiviral Responses through Suppression of Interferon-Stimulated Gene Transcription

Jing Ouyang, Xiaomei Zhu, Yuhai Chen, Haitao Wei, Qinghuang Chen, Xiaojuan Chi, Baomin Qi, Lianfeng Zhang, Yi Zhao, George Fu Gao, Guoshun Wang, and Ji-Long Chen

Supplemental Figures

Figure S1

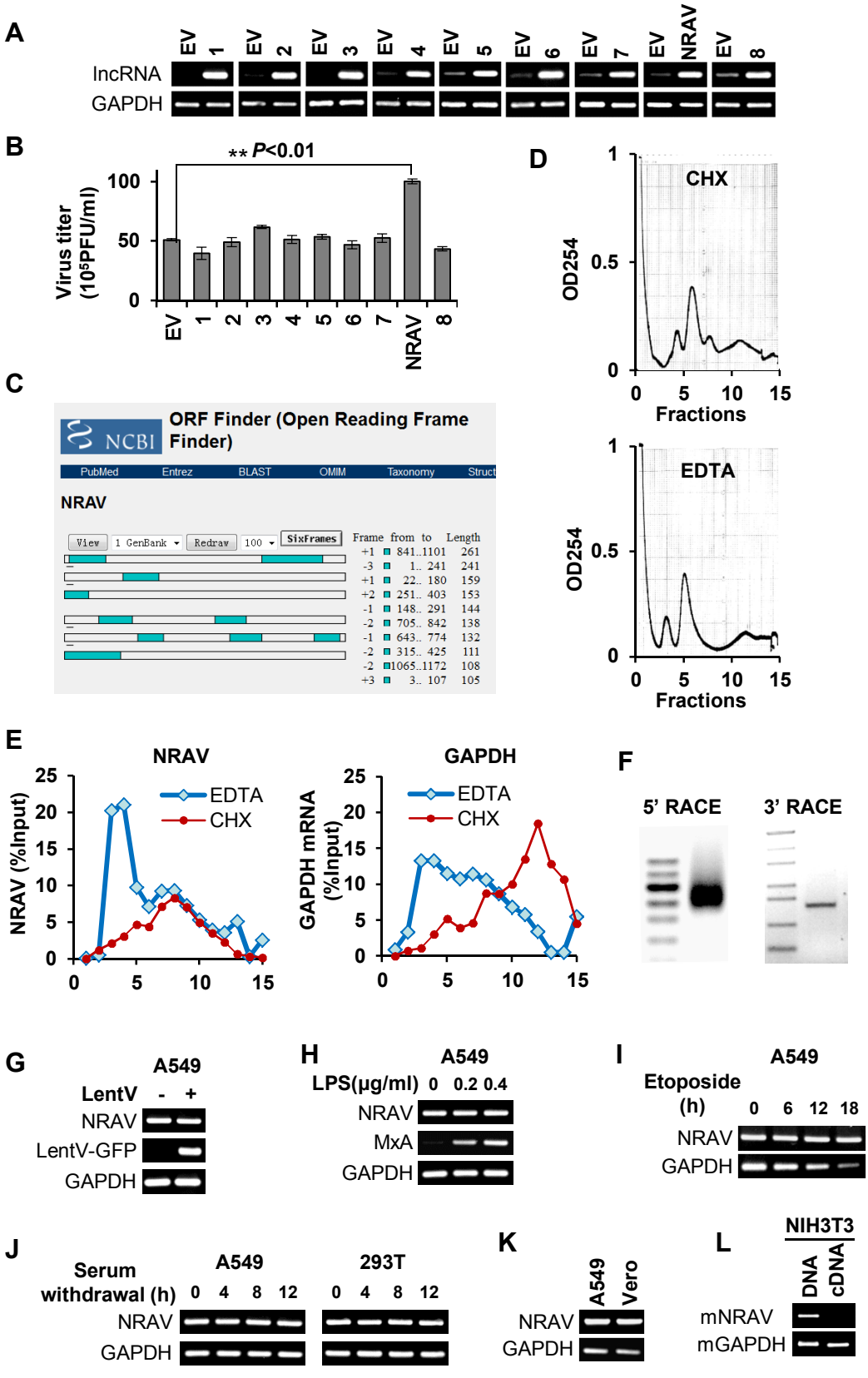

Figure S2

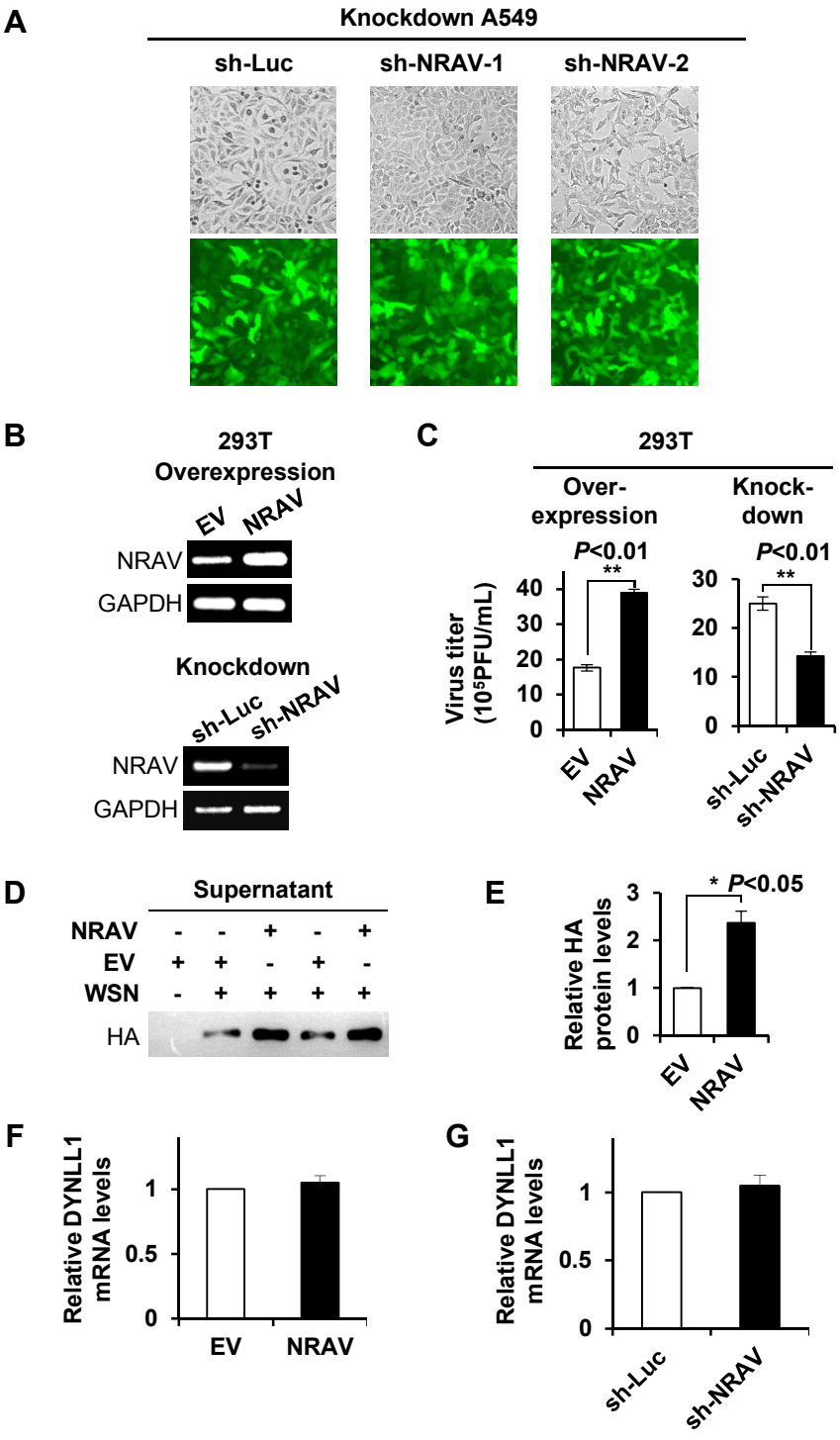
A
Knockdown A549
sh-Luc
sh-NRAV-1
sh-NRAV-2
B
293T
Overexpression
EV
NRAV
NRAV
GAPDH
Knockdown
sh-Luc
sh-NRAV
NRAV
GAPDH
C
293T
Over-expression
Knock-down
P<0.01
**
P<0.01
**
Virus titer (10^5PFU/mL)
40
30
20
10
0
30
20
10
0
EV
NRAV
sh-Luc
sh-NRAV
D
Supernatant
NRAV - - + - +
EV + + - + -
WSN - + + + +
HA
E
* P<0.05
Relative HA protein levels
3
2
1
0
EV
NRAV
F
Relative DYNLL1 mRNA levels
1
0.5
0
EV
NRAV
G
Relative DYNLL1 mRNA levels
1
0.5
0
sh-Luc
sh-NRAV

Figure S3

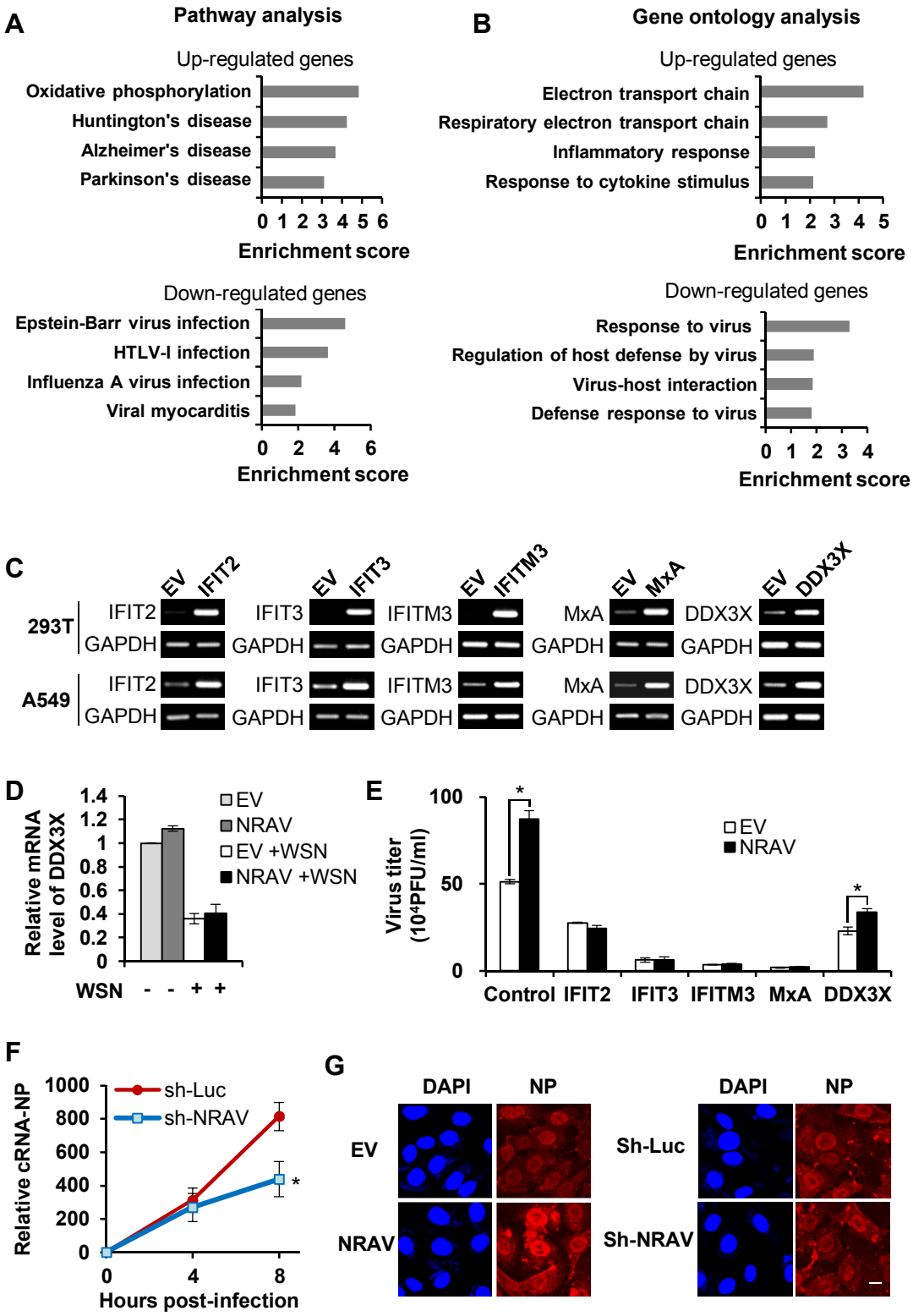
A
Pathway analysis
Up-regulated genes
Oxidative phosphorylation
Huntington's disease
Alzheimer's disease
Parkinson's disease
0 1 2 3 4 5 6
Enrichment score
Down-regulated genes
Epstein-Barr virus infection
HTLV-I infection
Influenza A virus infection
Viral myocarditis
0 2 4 6
Enrichment score
B
Gene ontology analysis
Up-regulated genes
Electron transport chain
Respiratory electron transport chain
Inflammatory response
Response to cytokine stimulus
0 1 2 3 4 5
Enrichment score
Down-regulated genes
Response to virus
Regulation of host defense by virus
Virus-host interaction
Defense response to virus
0 1 2 3 4
Enrichment score
C
EV
IFIT2
IFIT3
IFITM3
MxA
DDX3X
293T
A549
IFIT2
IFIT3
IFITM3
MxA
DDX3X
GAPDH
D
Relative mRNA level of DDX3X
1.4
1.2
1
0.8
0.6
0.4
0.2
0
EV
NRAV
EV +WSN
NRAV +WSN
WSN - - + +
E
Virus titer (10⁴PFU/ml)
100
50
0
EV
NRAV
*
*
Control IFIT2 IFIT3 IFITM3 MxA DDX3X
F
Relative cRNA-NP
1000
800
600
400
200
0
sh-Luc
sh-NRAV
*
0
4
8
Hours post-infection
G
DAPI
NP
EV
NRAV
Sh-Luc
Sh-NRAV

Figure S4

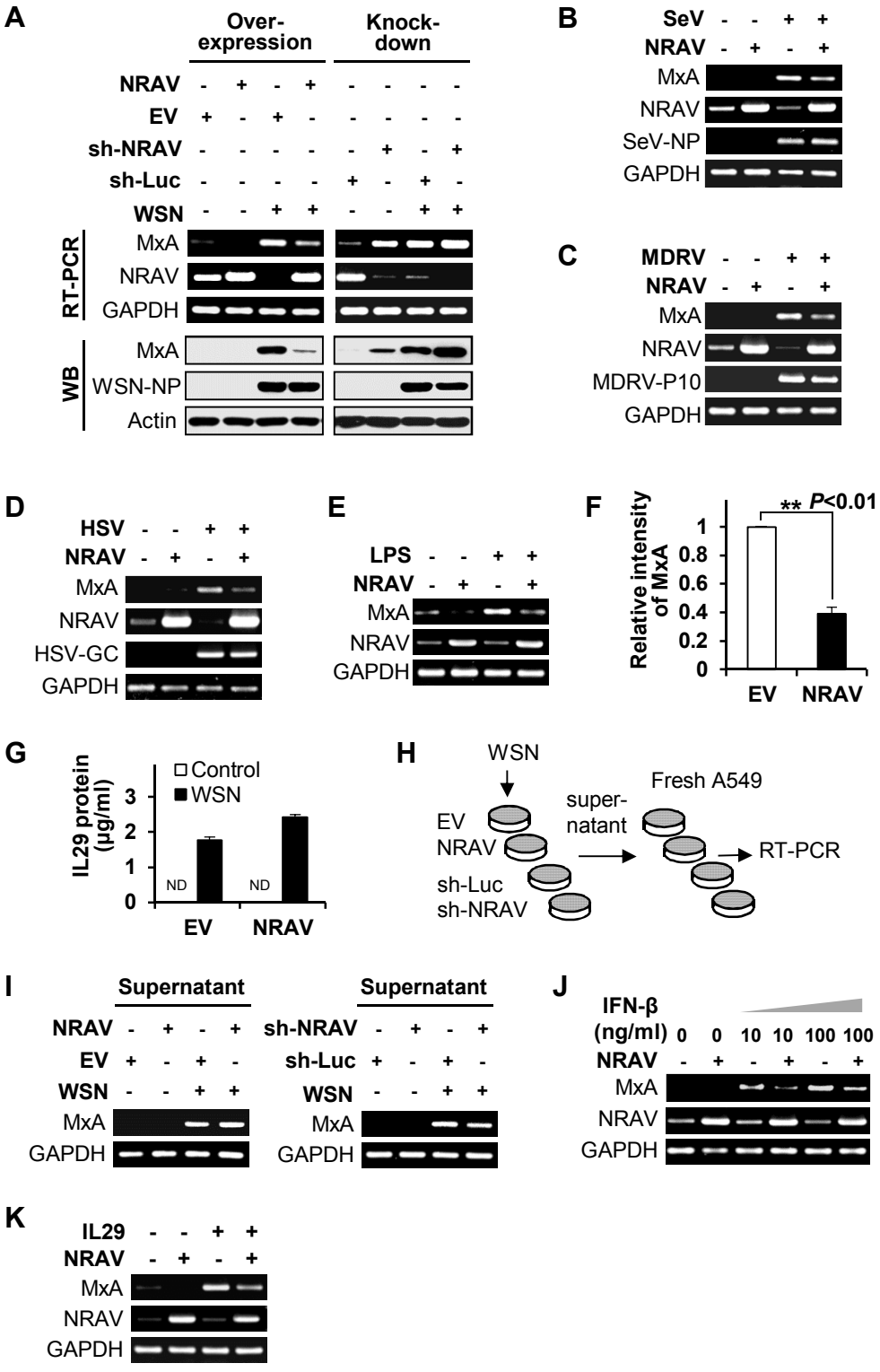
A
Over-expression
Knock-down
NRAV
EV
sh-NRAV
sh-Luc
WSN
RT-PCR
MxA
NRAV
GAPDH
WB
MxA
WSN-NP
Actin
B
SeV
NRAV
MxA
NRAV
SeV-NP
GAPDH
C
MDRV
NRAV
MxA
NRAV
MDRV-P10
GAPDH
D
HSV
NRAV
MxA
NRAV
HSV-GC
GAPDH
E
LPS
NRAV
MxA
NRAV
GAPDH
F
Relative intensity of MxA
** P<0.01
1
0.8
0.6
0.4
0.2
0
EV
NRAV
G
IL29 protein (μg/ml)
Control
WSN
3
2
1
0
ND
ND
EV
NRAV
H
WSN
Fresh A549
super-natant
EV
NRAV
sh-Luc
sh-NRAV
RT-PCR
I
Supernatant
Supernatant
NRAV
EV
WSN
sh-NRAV
sh-Luc
WSN
MxA
GAPDH
MxA
GAPDH
J
IFN-β (ng/ml)
0 0 10 10 100 100
NRAV
MxA
NRAV
GAPDH
K
IL29
NRAV
MxA
NRAV
GAPDH

Figure S5

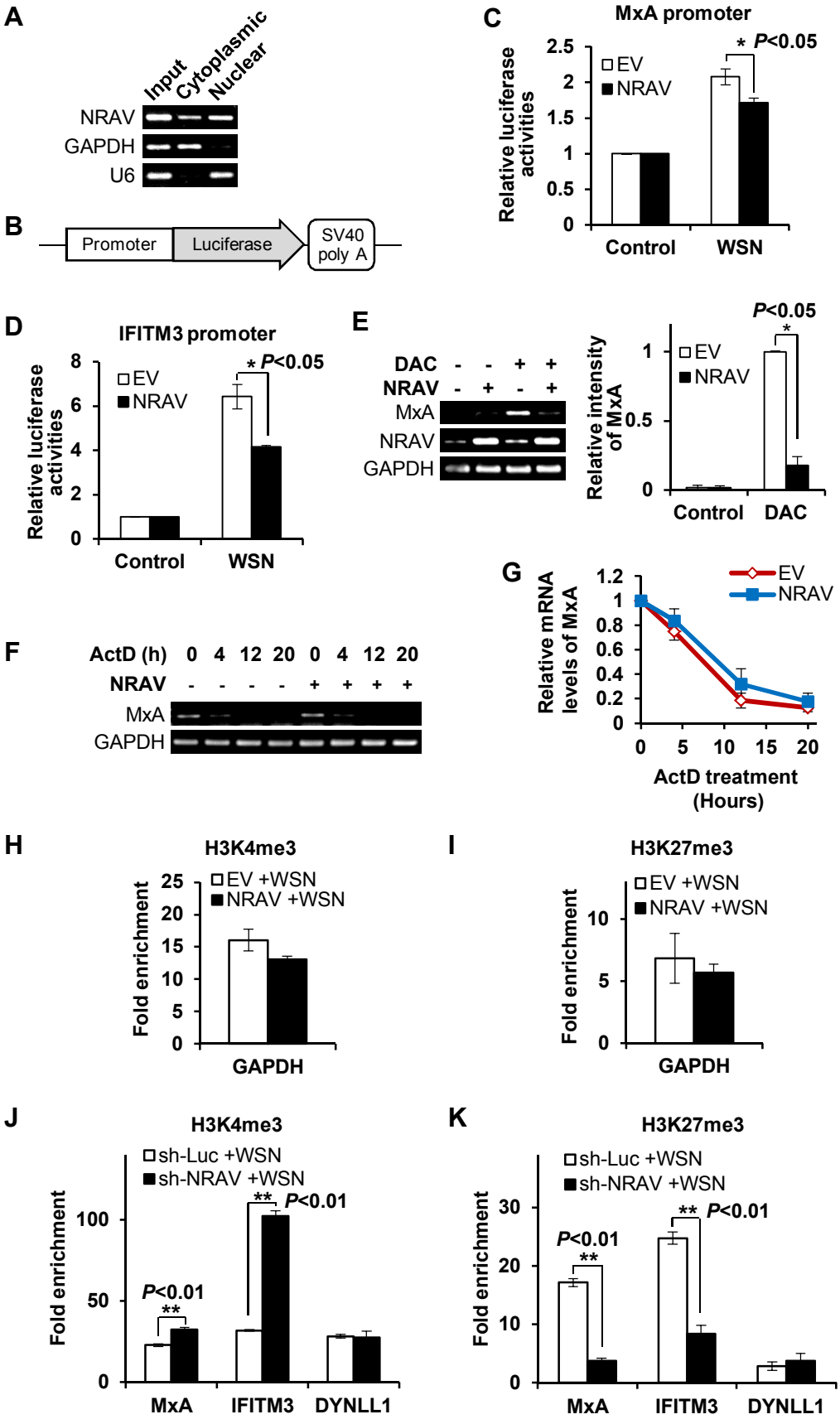
A
Input
Cytoplasmic
Nuclear
NRAV
GAPDH
U6
B
Promoter
Luciferase
SV40 poly A
C
MxA promoter
Relative luciferase activities
EV
NRAV
* P<0.05
Control
WSN
D
IFITM3 promoter
Relative luciferase activities
EV
NRAV
* P<0.05
Control
WSN
E
DAC - - + +
NRAV - + - +
MxA
NRAV
GAPDH
Relative intensity of MxA
EV
NRAV
P<0.05
*
Control
DAC
F
ActD (h) 0 4 12 20 0 4 12 20
NRAV - - - - + + + +
MxA
GAPDH
G
Relative mRNA levels of MxA
EV
NRAV
ActD treatment (Hours)
H
H3K4me3
Fold enrichment
EV +WSN
NRAV +WSN
GAPDH
I
H3K27me3
Fold enrichment
EV +WSN
NRAV +WSN
GAPDH
J
H3K4me3
Fold enrichment
sh-Luc +WSN
sh-NRAV +WSN
** P<0.01
** P<0.01
MxA
IFITM3
DYNLL1
K
H3K27me3
Fold enrichment
sh-Luc +WSN
sh-NRAV +WSN
P<0.01
**
** P<0.01
MxA
IFITM3
DYNLL1

Figure S6

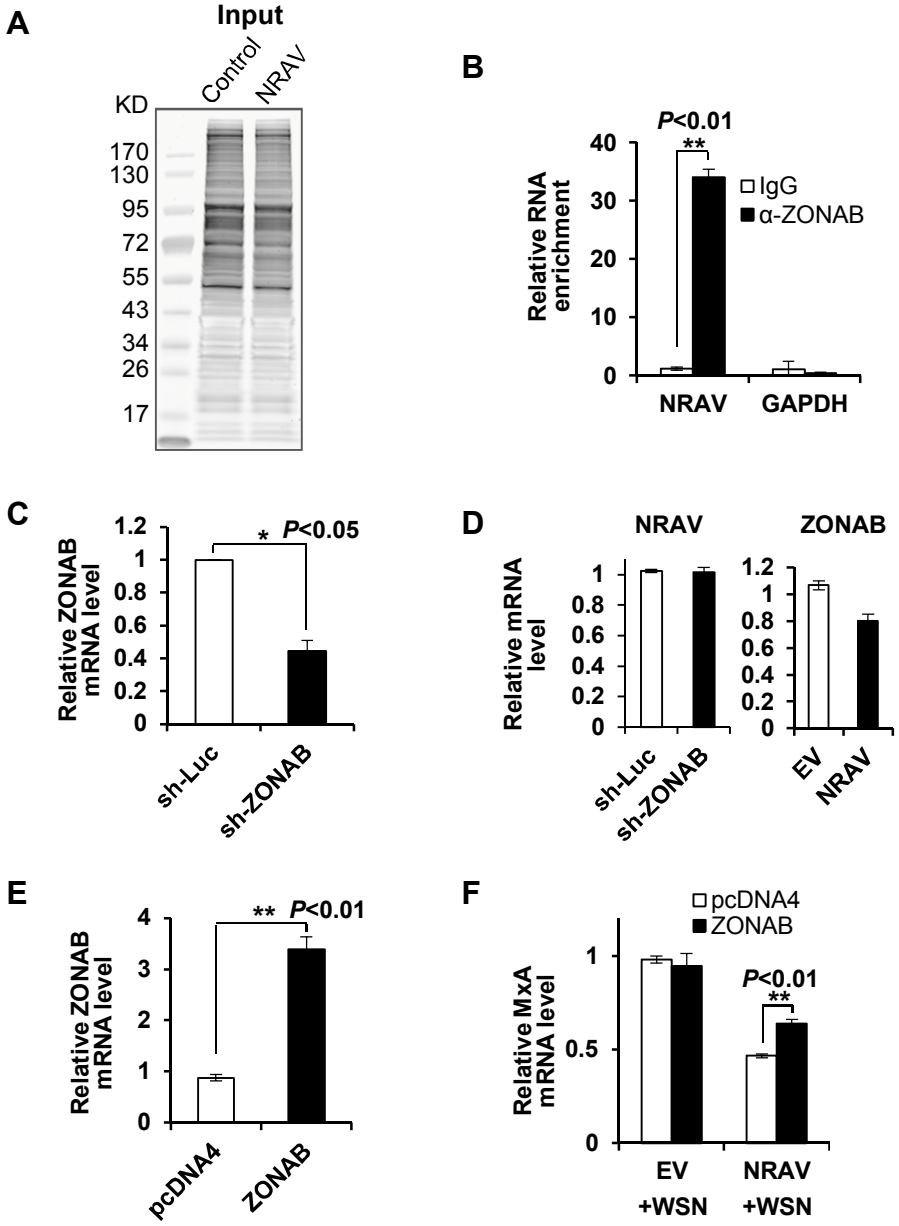
A
Input
Control
NRAV
KD
170
130
95
72
55
43
34
26
17
B
P<0.01
**
IgG
α-ZONAB
Relative RNA enrichment
40
30
20
10
0
NRAV
GAPDH
C
* P<0.05
Relative ZONAB mRNA level
1.2
1
0.8
0.6
0.4
0.2
0
sh-Luc
sh-ZONAB
D
NRAV
ZONAB
Relative mRNA level
1
0.8
0.6
0.4
0.2
0
1.2
1
0.8
0.6
0.4
0.2
0
sh-Luc
sh-ZONAB
EV
NRAV
E
** P<0.01
Relative ZONAB mRNA level
4
3
2
1
0
pcDNA4
ZONAB
F
pcDNA4
ZONAB
P<0.01
**
Relative MxA mRNA level
1
0.5
0
EV
+WSN
NRAV
+WSN

Figure S7

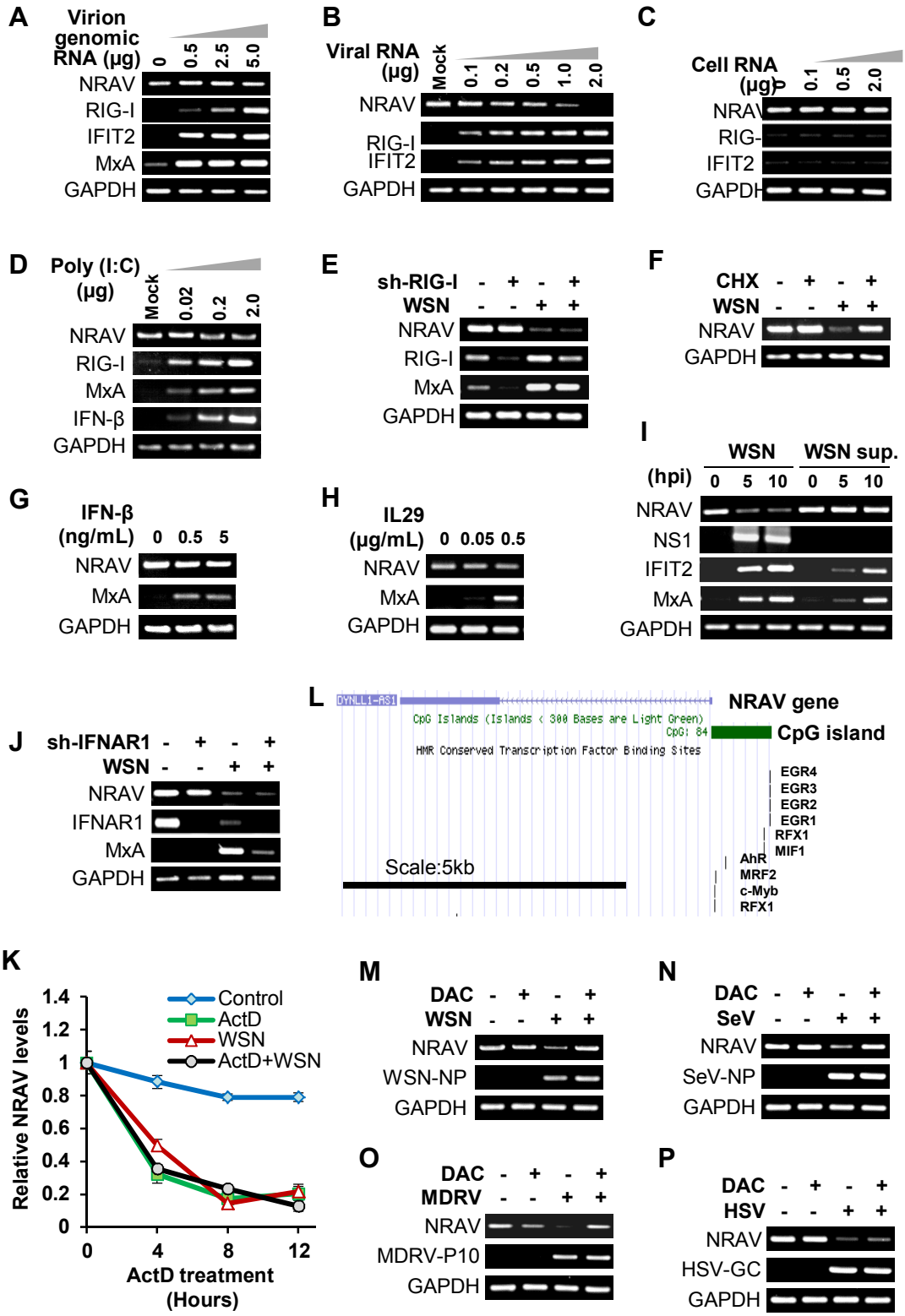
A
Virion genomic RNA (μg)
0 0.5 2.5 5.0
NRAV
RIG-I
IFIT2
MxA
GAPDH
B
Viral RNA (μg)
Mock 0.1 0.2 0.5 1.0 2.0
NRAV
RIG-I
IFIT2
GAPDH
C
Cell RNA (μg)
0 0.1 0.5 2.0
NRAV
RIG-I
IFIT2
GAPDH
D
Poly (I:C) (μg)
Mock 0.02 0.2 2.0
NRAV
RIG-I
MxA
IFN-β
GAPDH
E
sh-RIG-I - + - +
WSN - - + +
NRAV
RIG-I
MxA
GAPDH
F
CHX - + - +
WSN - - + +
NRAV
GAPDH
G
IFN-β (ng/mL) 0 0.5 5
NRAV
MxA
GAPDH
H
IL29 (μg/mL) 0 0.05 0.5
NRAV
MxA
GAPDH
I
WSN WSN sup.
(hpi) 0 5 10 0 5 10
NRAV
NS1
IFIT2
MxA
GAPDH
J
sh-IFNAR1 - + - +
WSN - - + +
NRAV
IFNAR1
MxA
GAPDH
L
DYNLL1-AS1
NRAV gene
CpG Islands (Islands < 300 Bases are Light Green)
CpG: 84
CpG island
HMR Conserved Transcription Factor Binding Sites
EGR4
EGR3
EGR2
EGR1
RFX1
MIF1
AhR
MRF2
c-Myb
RFX1
Scale:5kb
K
Relative NRAV levels
1.4
1.2
1
0.8
0.6
0.4
0.2
0
0 4 8 12
ActD treatment (Hours)
Control
ActD
WSN
ActD+WSN
M
DAC - + - +
WSN - - + +
NRAV
WSN-NP
GAPDH
N
DAC - + - +
SeV - - + +
NRAV
SeV-NP
GAPDH
O
DAC - + - +
MDRV - - + +
NRAV
MDRV-P10
GAPDH
P
DAC - + - +
HSV - - + +
NRAV
HSV-GC
GAPDH

Supplemental Information

Supplemental Figure Legends

Figure S1. Human NRAV Was Identified as a Functional LncRNA through Preliminary Functional Screening, Related to Figure 1

(A) The overexpression efficiencies of lncRNAs in A549 cells were determined by RT-PCR. Fragments of nine lncRNAs, indicated as 1 (BI832838), 2 (GD137531), 3 (D85245), 4 (BC107859), 5 (BX089654), 6 (uc001zcp), 7 (AY927564), NRAV (uc001tyk.1), and 8 (DA418630), amplified from A549 cells were used for ectopic expression as described in **Supplemental Experimental Procedures**.

(B) The lncRNA-overexpressing cells were infected with WSN (MOI=0.3) for 16 hours. The virus titers in culture supernatants were determined through plaque forming assay. Data from three independent experiments are expressed as means±s.e.m. $^{**}P<0.01$.

(C) LncRNA NRAV coding potential was predicted by ORF Finder as described in **Supplemental Experimental Procedures**. No ORF predicted (indicated in green) is longer than 300bp.

(D and E) Sucrose sedimentation and polysome analysis of the cytoplasmic fraction of A549. Cells incubated with cycloheximide (CHX) or mock were lysed as described in **Supplemental Experimental Procedures**. CHX-treated cell lysates were loaded on a 10-50% (weight to volume) sucrose gradient. The cytoplasmic fraction of CHX-untreated cells supplemented with 35 mM EDTA was also loaded on a sucrose gradient. After centrifugation, samples were fractionated from the top of the gradient

into 15 tubes while the absorbance at 254nm (OD254) was measured (D). RNA levels from each fraction were analyzed by qRT-PCR. Relative levels of NRAV (E, *left*) and GAPDH mRNA (E, *right*) are shown as %Input. Representative results from three independent experiments were shown.

(F) Agarose gel analysis of 5' and 3' RACE PCR products. DNA ladders (100, 200, 300, 400, 500,600, and 700 bp) are shown (left lane).

(G-J) A549 cells were transducted with pseudovirus (LentV) prepared by lentivirus expression system (G), or incubated with LPS (100 ng/ml, Invivogen) and sCD14 (300 ng/ml, PeproTech) for 8 h (H), or treated with etoposide (100 μM, Sigma) (I), or cultured in serum-free media for indicated time (J). The expression of NRAV were determined by RT-PCR.

(K) The expressions of NRAV in African green monkey kidney (Vero) cells and human A549 cells were detected by RT-PCR.

(L) The mouse DNA and cDNA prepared from NIH3T3 cells were used as templates to amplify mouse NRAV homolog (mNRAV).

These results shown are representative of at least three independent experiments.

Figure S2. Altering NRAV Expression Has Profound Effects on IAV Replication in Human Cells, Related to Figure 2

(A) Shown are representative phase and fluroscent images of NRAV knockdown A549 cells.

(B) The overexpression and knockdown of NRAV in 293T cells were determined by

RT-PCR. Representative results of three independent experiments are shown.

(C) Influenza virus replication was examined in NRAV-overexpressing and NRAV knockdown 293T cells by plaque forming assay as described in Figure 2E (MOI=0.3, *n*=3, means±s.e.m.) and **Supplemental Experimental Procedures**.

(D) IAV protein HA in supernatants from infected NRAV-overexpressing A549 cells (MOI=1) were detected by Western blotting. Supernatants of same volume at 16 hpi were collected and loaded parallelly. Representative results of three independent experiments are shown.

(E) The protein levels of HA in (D) lane 2 to lane5 were relatively quantitated by densitometry and normalized to GAPDH levels. In each experiment, the level of HA in infected EV control group is 1. Plotted are the average levels from three independent experiments (means±s.e.m.).

(F and G) The expression of DYNLL1 in NRAV-overexpression (F) and knockdown cells (G) were determined by qRT-PCR (*n*=3, means±s.e.m.).

Figure S3. NRAV Acts as a Negative Regulator to Modulate the Expression of Several Key ISGs, Related to Figure 4

(A and B) Pathway analysis (A) and Gene Ontology analysis (B) of up-regulated genes (*upper*) and down-regulated genes (*lower*) from microarray data indicated that many decreased genes were associated with viral infection or host response to virus. Enrichment score is calculated as $-\log_{10}$ (*P*-value), and *P*-value is calculated by Fisher's exact test.

(C) The transient expression of exogenous human IFIT2, IFIT3, IFITM3, MxA or DDX3X in experiments was determined by RT-PCR at 24 hours post-transfection. For each experiment, 1 μg expression plasmid is used for transfection (6 well plate). Representative results of three independent experiments are shown.

(D) The DDX3X mRNA levels in NRAV and EV cells were measured by qRT-PCR (n=3, means±s.e.m.), which was not significantly affected by NRAV overexpression.

(E) Transient expressions of ISGs were performed in NRAV-overexpressing cells or EV cells as described in **Supplemental Experimental Procedures**. 24 hours after transfection, cells were infected with IAV for 16 hours. The virus titers were determined by plaque forming assay (n=3). The empty plasmid was used as control, as well as the expression plasmid of DDX3X.

(F) Viral cRNA of WSN-NP in infected NRAV knockdown cells (MOI=1) were detected by qRT-PCR. Data are shown as means±s.e.m. (n=3). *P< 0.05.

(G) A549 cells stably expressing NRAV or sh-NRAV or controls were incubated with WSN virus (MOI=100) on ice, and then cultured with warm media for 4 h. Immunofluorescence staining was performed using an anti-NP antibody to detect entry of NP (red). The nuclei were stained with DAPI (blue). Scale bar, 10 μm.

Figure S4. NRAV Suppresses the Transcription of MxA without Affecting IFN Signaling, Related to Figure 5

(A) The MxA mRNA (upper) and protein (lower) levels in NRAV-overexpressing or NRAV knockdown cells infected or uninfected with WSN (MOI=3) were measured

by RT-PCR and Western blotting, respectively. Empty vector or sh-Luc expressing plasmid are used as control.

(B-D) The MxA mRNA levels in following NRAV-overexpressing cells or EV control cells were determined by RT-PCR: SeV infected A549 cells (B), MDRV infected 293T cells (C), and HSV infected A549 cells (D). Representative results of three independent experiments are shown.

(E) The MxA mRNA levels in NRAV-overexpressing cells or EV control cells stimulated by LPS (100 ng/ml) and sCD14 (300 ng/ml) were determined by RT-PCR.

(F) Levels of MxA mRNA in (E) lane 3 and lane 4 were quantitated by densitometry as described in Figure S2E. Plotted are the average levels from three independent experiments (means±s.e.m.).

(G) The IL29 protein levels in supernatants of EV and NRAV cells infected with or without WSN (MOI=1) were analyzed by ELISA. Data are shown as means±s.e.m. n=3.

(H) Experimental schematic of cytokine assay. NRAV-overexpressing or NRAV knockdown A549 cells and control cells were infected with or without WSN (MOI=1). The supernatants of above cells were collected at 8 hpi and used to incubate the fresh A549 cells for 1.5 hours.

(I) The MxA mRNA levels in supernanant-incubated cells described in (H) were assessed by RT-PCR. Representative results of three independent experiments are shown.

(J and K) The MxA mRNA levels in NRAV-overexpressing cells and control cells

stimulated by IFN-β (J) or IL29 (K) (50 ng/ml) respectively for 3 h were detected by RT-PCR . Representative results of three independent experiments are shown.

Cells were infected or stimulated as described in **Experimental Procedures.** Data are shown as means±s.e.m. n=3. *P<0.05, **P<0.01.

Figure S5. NRAV Regulates Promoter Activities and Histone Modifications of ISGs, Related to Figure 6

(A) The RNA levels of NRAV, cytoplasmic control transcript (GAPDH mRNA) and nuclear control transcript (U6 RNA) were assessed by RT-PCR in cytoplasmic and nuclear fractions from A549. The total cells were used as input control.

(B) Shown is the schematic diagram of the plasmid construct for luciferase gene reporter assay.

(C and D) 293T cells overexpressing NRAV or EV control were transfected with pGL3-MxAP-Luc (C) or pGL3-IFITM3P-Luc (D) in combination with pRL-TK for 10 h and then infected with WSN for 12 h as described in **Supplemental Experimental Procedures**. Luciferase activity in cell lysates was measured and displayed as mean±s.e.m. of relative luciferase units normalized to Renilla luciferase activity from three independent experiments.

(E) A549 cells overexpressing NRAV were treated with 10 μM decitabine (DAC) as described in **Supplemental Experimental Procedures** and infected with WSN (MOI=3) for 12 h. The mRNA levels of MxA were detected by RT-PCR (*left*). Levels of MxA mRNA were relatively quantitated by densitometry (*right*) as described in

Figure S2E. Plotted are the average levels from three independent experiments.

(F and G) A549 cells overexpressing NRAV were infected with WSN and treated with 2.5 μg/ml actinomycin D (ActD) as described in **Supplemental Experimental Procedures**. Cells were collected at 0, 4, 12, 20 h time points. The mRNA levels of MxA were detected by RT-PCR (F) and qRT-PCR (G).

(H and I) ChIP analysis of H3K4me3 (H) and H3K27me3 (I) levels at the *gapdh* locus in infected NRAV-overexpressing or control A549 cells as described in Figure 6F and **Supplemental Experimental Procedures**.

(J and K) ChIP analysis of H3K4me3 (J) and H3K27me3 (K) levels at the *mxA,ifitm3* and *dynll1* locus in infected NRAV knockdown or control A549 cells.

Representative results of three independent RT-PCR experiments are shown. Data of are shown as means±s.e.m. (n=3, *P<0.05, **P<0.01).

Figure S6. Interaction between NRAV and ZONAB and the Function of ZONAB on MxA Transcription, Related to Figure 6

(A) Silver staining of input proteins of RNA pulldown assay as described in Figure 6H and **Supplemental Experimental Procedures**. Shown is representative result from three independent experiments.

(B) The association of NRAV with ZONAB is verified by RNA immunoprecipitation (RIP). Uninfected cell lysates were immunoprecipitated with anti-ZONAB Ab or control IgG as described in **Supplemental Experimental Procedures**. The enrichments of NRAV or GAPDH mRNA were analyzed by qRT-PCR and

normalized to input and control IgG. The fold enrichment was calculated as $2^{(-\Delta\Delta Ct)}$.

(C) ZONAB was depleted by shRNA sequences through transient transfection with A549 cells. ZONAB mRNA levels were measured by qRT-PCR and normalized to that of control sh-Luc cells.

(D) NRAV expression in ZONAB depleted cells (*left*) as described in (C) and ZONAB mRNA levels in NRAV-overexpressing A549 cells (*right*) were determined by qRT-PCR and normalized to that of control sh-Luc/EV cells respectively.

(E) ZONAB isoform b was transiently expressed in A549 cells by transfecting with transient expression plasmid containing ZONAB isoform b ORF. The mRNA levels were measured by qRT-PCR and normalized to that of control cells transfected with empty vector pcDNA4.

(F) MxA mRNA levels in IAV-infected NRAV-overexpressing A549 cells and EV control cells transfected with transient expression plasmids containing ZONAB isoform b ORF or empty vector pcDNA4 were determined by qRT-PCR and normalized to that of infected EV cells transfected with pcDNA4.

Data are shown as means±s.e.m. (n=3. *P<0.05, **P<0.01).

Figure S7. Down-regulation of NRAV Is Dependent on Virus Replication, Protein Synthesis and Epigenetic Regulation, Related to Figure 6 and Discussion

RT-PCR was performed to examine the RNA expression in following A549 cells:

(A-D) Cells were transfected with WSN virion genomic RNA (A), viral RNA isolated from WSN infected cells (B), cellular RNA derived from uninfected cells (C) and

poly(I:C) (D) of indicated amount for 4 hours. IAV genomic RNA could not affect the NRAV level. By contrast, transfection with viral RNA from IAV infected cells caused marked reduction in NRAV expression. The treatment with poly(I:C) had no effect on NRAV expr ession.

(E) RIG-I knockdown A549 cells generated using specific shRNA targeting RIG-I as described in **Supplemental Experimental Procedures** were infected with WSN. The depletion of RIG-I had no effect on NRAV expression.

(F) Cells were treated with 1μg/ml cycloheximide (CHX) for 30 min before WSN infection. The NRAV level recovered greatly in CHX-pretreated and WSN-infected cells.

(G-I) Cells were stimulated with cytokines IFN-β (G), IL29 (type III IFN) (H) of indicated amount or incubated with culture supernatant (sup.) collected from infected cells (I) for 4 hours. In (I), infected cells were used as control. These virus-induced cytokines could not affect the NRAV level.

(J) The type I IFN receptor IFNAR1 knockdown cells generated using specific shRNA (Invivogen) were infected with WSN. The depletion of IFNAR1 had no effect on NRAV expression.

(K) NRAV RNA decay assay was performed with actinomycin (ActD) treatment of A549 cells infected with WSN (MOI=3) or not. Cells were collected at 0, 4, 8, 12h time points and the NRAV levels were determined by qRT-PCR described in **Supplemental Experimental Procedures (**means±s.e.m. n=3). The turnover rate of NRAV in infected cells did not show difference with that in uninfected cells.

(L) Predicted CpG island in NRAV promoter region and binding sites of transcription factors are shown. Prediction data were from UCSC genome browser database (February 2009 human reference sequence (GRCh37), http://genome.ucsc.edu). Scale bar: 5kb.

(M-P) Cells were treated with 10 μM DNA methyltransferase inhibitor decitabine (DAC) for 2 days before infection with WSN (M), SeV (N), MDRV (O) and HSV (P) as described in **Supplemental Experimental Procedures.** Shown are representative results from three independent experiments. The NRAV levels were obviously recovered in cells pretreated with DAC and infected with IAV, SeV, and MDRV, but less significant in DNA virus HSV infected cells.

Table S1. Full-length sequence of NRAV, Related to Figure 1

NRAV
GGGCAATGGGCCGCACGCTACGAGGCCCACACACCCAGAAGGTGGAGCCCCGGCCGGGTT
ACGCGGACCACCCAGCTGTCTGGAGAGATGAAGAAAATGAGGTTCAAAGAGATGAAGTCT
CTTGCCTAAAGTCAGTGACAGAAAGTGACAGAGCTGGGATGTGAATCCTGGTCTGACTCTA
CAGTCCCACATGGTAGATGGAACCTCCGAGCAACACCTAAACAAAGGGAGTTGATGCCTCC
GAACAGAGTAATGTCGCTGGAGACACTAAGCATCGTCGGCCCCTGGCAGGAGCTCCCTAAA
TATGTGTTGGATGGATGGAAGAAAGGATGGATAGTTCAGAGTACTTCAGCCTTGATTCCTCC
GCAACAGACACCTGAAACTTGACCCTACATTGGTTCTTGGCCATCGTGATCTTCCTTGGACA
GAATCACCTTTCAGCTCCGGTCATCAGACTTTCCCAGGGCCCTCAGAAAGCCCTTCAGAGT
TGTTACTCACAGGCAGGCTGAGGGATTCCTTACGGGGTCTGCAGCTCTCCTCACCTCATCCA
CAAGTAGGACCGTGGCCTGTTCCTCACTACTGCCCCAGGATCACTCTGTTCCCAGCCCAGT
CCAGCAATCACTTGTCTAGCTTTCTGGAACCTTGAGTACTTTCTTGAACCATGAGTCCTGTG
ACCACCCTAGCAGCTCTAACCCTCCCTTATCTGAAAGGAAGTGTGAGGTGACCTTGCAGGT
CCCAGAGTTGATTGAAGACCCCATCCAGAAAGAAGGCACCCTGTGGGAGAGATTGCAAGG
CCTAGGTCTGAATCCGGAAGCTTCCACCCCATGGAGAAGGGCTGGCACCAGCCTGGGGCT
GGCAGTGGAGCTGAGCTTTGGAGCCAAGGACTGTACTGCAGTGCAGGGAGAGTGAGGCCA
GAAAGGCTGAGACAACTCAGGGAAAGAAAACCTCCCTTCTGGCTAATAGTCAAGCACCGC
CTGAGTAGACCAACACTCTCCTGTCCACAGGGGCAGCAGATGAAGACACAACCAGAGAGG
ACTAACAGGCCCCCTCAGCTCTCAGTCAGAGGGCAGAGCAACACAGAATAGACATTAAAG
GAACAGACTTTGAGGCCAGGCAGCCTTGGGTGTGCATCTGTCCCTACTAAGCCATGTGACA
TTAAACAAGTGAGTCCACCTCAAAAAAAAAAAA

The full-length sequence of NRAV is combined the end sequences of NRAV determined by 5’ and 3’ RACE and the middle fragment sequence of NRAV cloned from cDNAs of A549 cells by RT-PCR.

Table S2. ISGs Differentially Expressed in NRAV-overexpressing Cells, Related to Figure 4

Down-regulated ISGs

Entrez Gene ID	Gene Symbol	Description
3433	IFIT2	Interferon-induced protein with tetratricopeptide repeats 2 (IFIT-2) (Interferon-induced 54 kDa protein) (IFI-54K) (ISG-54 K). [Source:Uniprot/SWISSPROT;Acc:P09913]
3437	IFIT3	Interferon-induced protein with tetratricopeptide repeats 3 (IFIT-3) (IFIT-4) (Interferon-induced 60 kDa protein) (IFI-60K) (ISG-60) (CIG49) (Retinoic acid-induced gene G protein) (RIG-G). [Source:Uniprot/SWISSPROT;Acc:O14879]
144383	IFITM3	Interferon-induced transmembrane protein 3 (Interferon-inducible protein 1-8U). [Source:Uniprot/SWISSPROT;Acc:Q01628]
8638	OASL	59 kDa 2-5-oligoadenylate synthetase-like protein (p59 OASL) (p59OASL) (Thyroid receptor-interacting protein 14) (TRIP-14). [Source:Uniprot/SWISSPROT;Acc:Q15646]
4599	MX1	Interferon-induced GTP-binding protein Mx1 (Interferon-regulated resistance GTP-binding protein MxA) (Interferon-induced protein p78) (IFI-78K). [Source:Uniprot/SWISSPROT;Acc:P20591]
58	ACTA1	Actin, alpha skeletal muscle (Alpha-actin-1). [Source:Uniprot/SWISSPROT;Acc:P68133]
8125	ANP32A	Acidic leucine-rich nuclear phosphoprotein 32 family member A (Potent heat-stable protein phosphatase 2A inhibitor I1PP2A) (Acidic nuclear phosphoprotein pp32) (Leucine-rich acidic nuclear protein) (Lanp) (Putative HLA-DR-associated protein I) (PHAPI)
9582	APOBEC3B	Probable DNA dC->dU-editing enzyme APOBEC-3B (EC 3.5.4.-) (Phorbolin- 1-related protein) (Phorbolin-2/3). [Source:Uniprot/SWISSPROT;Acc:Q9UH17]
23780	APOL2	Apolipoprotein-L2 (Apolipoprotein L-II) (ApoL-II). [Source:Uniprot/SWISSPROT;Acc:Q9BQE5]
808	CALM3	Calmodulin (CaM). [Source:Uniprot/SWISSPROT;Acc:P62158]
824	CAPN2	Calpain-2 catalytic subunit precursor (EC 3.4.22.53) (Calpain-2 large subunit) (Calcium-activated neutral proteinase 2) (CANP 2) (Calpain M-type) (M-calpain) (Millimolar-calpain) (Calpain large polypeptide L2). [Source:Uniprot/SWISSPROT;Acc:P17655]
6352	CCL5	Small inducible cytokine A5 precursor (CCL5) (T-cell-specific RANTES protein) (SIS-delta) (T cell-specific protein P228) (TCP228) [Contains: RANTES(3-68); RANTES(4-68)]. [Source:Uniprot/SWISSPROT;Acc:P13501]
894	CCND2	G1/S-specific cyclin-D2. [Source:Uniprot/SWISSPROT;Acc:P30279]
972	CD74	HLA class II histocompatibility antigen gamma chain (HLA-DR antigens- associated invariant chain) (Ia antigen-associated invariant chain) (Ii) (p33) (CD74 antigen). [Source:Uniprot/SWISSPROT;Acc:P04233]
991	CDC20	Cell division cycle protein 20 homolog (p55CDC). [Source:Uniprot/SWISSPROT;Acc:Q12834]
1026	CDKN1A	Cyclin-dependent kinase inhibitor 1 (p21) (CDK-interacting protein 1) (Melanoma differentiation-associated protein 6) (MDA-6). [Source:Uniprot/SWISSPROT;Acc:P38936]
7812	CSDE1	Cold shock domain-containing protein E1 (UNR protein) (N-ras upstream gene protein). [Source:Uniprot/SWISSPROT;Acc:O75534]
1520	CTSS	Cathepsin S precursor (EC 3.4.22.27). [Source:Uniprot/SWISSPROT;Acc:P25774]
1832	DSP	Desmoplakin (DP) (250/210 kDa paraneoplastic pemphigus antigen). [Source:Uniprot/SWISSPROT;Acc:P15924]

1843	DUSP1	Dual specificity protein phosphatase 1 (EC 3.1.3.48) (EC 3.1.3.16) (MAP kinase phosphatase 1) (MKP-1) (Protein-tyrosine phosphatase CL100) (Dual specificity protein phosphatase hVH1). [Source:Uniprot/SWISSPROT;Acc:P28562]
10682	EBP	3-beta-hydroxysteroid-Delta(8),Delta(7)-isomerase (EC 5.3.3.5) (Cholestenol Delta-isomerase) (Delta(8)-Delta(7) sterol isomerase) (D8-D7 sterol isomerase) (Emopamil-binding protein). [Source:Uniprot/SWISSPROT;Acc:Q15125]
1975	EIF4B	Eukaryotic translation initiation factor 4B (eIF-4B). [Source:Uniprot/SWISSPROT;Acc:P23588]
2048	EPHB2	Ephrin type-B receptor 2 precursor (EC 2.7.10.1) (Tyrosine-protein kinase receptor EPH-3) (DRT) (Receptor protein-tyrosine kinase HEK5) (ERK) (Tyrosine-protein kinase TYRO5) (Renal carcinoma antigen NY-REN- 47). [Source:Uniprot/SWISSPROT;Acc:P29323]
3170	FOXA2	Hepatocyte nuclear factor 3-beta (HNF-3B) (Forkhead box protein A2). [Source:Uniprot/SWISSPROT;Acc:Q9Y261]
2294	FOXF1	Forkhead box protein F1 (Forkhead-related protein FKHL5) (Forkhead- related transcription factor 1) (FREAC-1) (Forkhead-related activator 1). [Source:Uniprot/SWISSPROT;Acc:Q12946]
23710	GABARAPL3	Gamma-aminobutyric acid receptor-associated protein-like 1 (GABA(A) receptor-associated protein-like 1) (Glandular epithelial cell protein 1) (GEC-1) (Early estrogen-regulated protein). [Source:Uniprot/SWISSPROT;Acc:Q9H0R8]
2821	GPI	Glucose-6-phosphate isomerase (EC 5.3.1.9) (GPI) (Phosphoglucose isomerase) (PGI) (Phosphohexose isomerase) (PHI) (Neuroleukin) (NLK) (Sperm antigen 36) (SA-36). [Source:Uniprot/SWISSPROT;Acc:P06744]
2987	GUK1	Guanylate kinase (EC 2.7.4.8) (GMP kinase). [Source:Uniprot/SWISSPROT;Acc:Q16774]
3054	HCFC1	Host cell factor (HCF) (HCF-1) (C1 factor) (VP16 accessory protein) (VCAF) (CFF)
3105	HLA-A	HLA class I histocompatibility antigen, A-3 alpha chain precursor (MHC class I antigen A*3). [Source:Uniprot/SWISSPROT;Acc:P04439]
730410	1B18_HUMAN	HLA class I histocompatibility antigen, B-18 alpha chain precursor (MHC class I antigen B*18). [Source:Uniprot/SWISSPROT;Acc:P30466]
3107	1C07_HUMAN	HLA class I histocompatibility antigen, Cw-7 alpha chain precursor (MHC class I antigen Cw*7). [Source:Uniprot/SWISSPROT;Acc:P10321]
3133	NP_005507.3	major histocompatibility complex, class I, E precursor [Source:RefSeq_peptide;Acc:NP_005507]
3135	HLA-G	HLA class I histocompatibility antigen, alpha chain G precursor (HLA G antigen). [Source:Uniprot/SWISSPROT;Acc:P17693]
7184	HSP90B1	Endoplasmin precursor (Heat shock protein 90 kDa beta member 1) (94 kDa glucose-regulated protein) (GRP94) (gp96 homolog) (Tumor rejection antigen 1). [Source:Uniprot/SWISSPROT;Acc:P14625]
8870	NP_003888.2	immediate early response 3 [Source:RefSeq_peptide;Acc:NP_003888]
3460	IFNGR2	Interferon-gamma receptor beta chain precursor (Interferon-gamma receptor accessory factor 1) (AF-1) (Interferon-gamma transducer 1). [Source:Uniprot/SWISSPROT;Acc:P38484]
3576	IL8	Interleukin-8 precursor (IL-8) (CXCL8) (Monocyte-derived neutrophil chemotactic factor) (MDNCF) (T-cell chemotactic factor) (Neutrophil- activating protein 1) (NAP-1) (Protein 3-10C) (Granulocyte chemotactic protein 1) (GCP-1)
3693	ITGB5	Integrin beta-5 precursor. [Source:Uniprot/SWISSPROT;Acc:P18084]
3959	LGALS3BP	Galectin-3-binding protein precursor (Lectin galactoside-binding soluble 3-binding protein) (Mac-2-binding protein) (Mac-2 BP) (MAC2BP) (Tumor-associated antigen 90K). [Source:Uniprot/SWISSPROT;Acc:Q08380]

4061	LY6E	Lymphocyte antigen 6E precursor (Ly-6E) (Retinoic acid-induced gene E protein) (RIG-E) (Thymic shared antigen 1) (TSA-1) (Stem cell antigen 2) (SCA-2). [Source:Uniprot/SWISSPROT;Acc:Q16553]
65108	MARCKSL1	MARCKS-related protein (MARCKS-like protein 1) (Macrophage myristoylated alanine-rich C kinase substrate) (Mac-MARCKS) (MacMARCKS). [Source:Uniprot/SWISSPROT;Acc:P49006]
4605	MYBL2	Myb-related protein B (B-Myb). [Source:Uniprot/SWISSPROT;Acc:P10244]
4771	NF2	Merlin (Moesin-ezrin-radixin-like protein) (Neurofibromin-2) (Schwannomin) (Schwannomerlin). [Source:Uniprot/SWISSPROT;Acc:P35240]
652607	PABPC1	Polyadenylate-binding protein 1 (Poly(A)-binding protein 1) (PABP 1). [Source:Uniprot/SWISSPROT;Acc:P11940]
84333	PCGF5	Polycomb group RING finger protein 5 (RING finger protein 159). [Source:Uniprot/SWISSPROT;Acc:Q86SE9]
5111	PCNA	Proliferating cell nuclear antigen (PCNA) (Cyclin). [Source:Uniprot/SWISSPROT;Acc:P12004]
5329	PLAUR	Urokinase plasminogen activator surface receptor precursor (uPAR) (U- PAR) (Monocyte activation antigen Mo3) (CD87 antigen). [Source:Uniprot/SWISSPROT;Acc:Q03405]
5359	PLSCR1	Phospholipid scramblase 1 (PL scramblase 1) (Ca(2+)-dependent phospholipid scramblase 1) (Erythrocyte phospholipid scramblase) (MmTRA1b). [Source:Uniprot/SWISSPROT;Acc:O15162]
5432	POLR2C	DNA-directed RNA polymerase II subunit RPB3 (RNA polymerase II subunit B3) (RNA polymerase II subunit 3) (DNA-directed RNA polymerase II subunit C) (DNA-directed RNA polymerase II 33 kDa polypeptide) (RPB33) (RPB31). [Source:Uniprot/SWISSPROT;Acc:P19387]
5445	PON2	Serum paraoxonase/arylesterase 2 (EC 3.1.1.2) (EC 3.1.8.1) (PON 2) (Serum aryldialkylphosphatase 2) (A-esterase 2) (Aromatic esterase 2). [Source:Uniprot/SWISSPROT;Acc:Q15165]
5473	PPBP	Platelet basic protein precursor (PBP) (Small inducible cytokine B7) (CXCL7) (Leukocyte-derived growth factor) (LDGF) (Macrophage-derived growth factor) (MDGF)
5514	PPP1R10	Serine/threonine-protein phosphatase 1 regulatory subunit 10 (Phosphatase 1 nuclear targeting subunit) (MHC class I region proline- rich protein CAT53) (FB19 protein) (PP1-binding protein of 114 kDa) (p99). [Source:Uniprot/SWISSPROT;Acc:Q96QC0]
5836	PYGL	Glycogen phosphorylase, liver form (EC 2.4.1.1). [Source:Uniprot/SWISSPROT;Acc:P06737]
5880	RAC2	Ras-related C3 botulinum toxin substrate 2 precursor (p21-Rac2) (Small G protein) (GX). [Source:Uniprot/SWISSPROT;Acc:P15153]
5935	RBM3	Putative RNA-binding protein 3 (RNA-binding motif protein 3) (RNPL). [Source:Uniprot/SWISSPROT;Acc:P98179]
389	RHOC	Rho-related GTP-binding protein RhoC precursor (H9). [Source:Uniprot/SWISSPROT;Acc:P08134]
6124	RPL4	60S ribosomal protein L4 (L1). [Source:Uniprot/SWISSPROT;Acc:P36578]
6175	RPLP0	60S acidic ribosomal protein P0 (L10E). [Source:Uniprot/SWISSPROT;Acc:P05388]
91543	RSAD2	radical S-adenosyl methionine domain containing 2 [Source:RefSeq_peptide;Acc:NP_542388]
5054	SERPINE1	Plasminogen activator inhibitor 1 precursor (PAI-1) (Endothelial plasminogen activator inhibitor) (PAI). [Source:Uniprot/SWISSPROT;Acc:P05121]
29946	SERTAD3	SERTA domain-containing protein 3 (Replication protein-binding trans- activator) (RPA-binding trans-activator). [Source:Uniprot/SWISSPROT;Acc:Q9UJW9]
6774	STAT3	Signal transducer and activator of transcription 3 (Acute-phase response factor). [Source:Uniprot/SWISSPROT;Acc:P40763]
7040	TGFB1	Transforming growth factor beta-1 precursor (TGF-beta-1) [Contains: Latency-associated peptide

		(LAP)]. [Source:Uniprot/SWISSPROT;Acc:P01137]
7083	TK1	Thymidine kinase, cytosolic (EC 2.7.1.21). [Source:Uniprot/SWISSPROT;Acc:P04183]
4071	TM4SF1	Transmembrane 4 L6 family member 1 (Tumor-associated antigen L6) (Membrane component surface marker 1) (M3S1). [Source:Uniprot/SWISSPROT;Acc:P30408]
7127	TNFAIP2	Tumor necrosis factor, alpha-induced protein 2 (Primary response gene B94 protein). [Source:Uniprot/SWISSPROT;Acc:Q03169]
9322	TRIP10	Cdc42-interacting protein 4 (Thyroid receptor-interacting protein 10) (TRIP-10) (Protein Felic) (Salt-tolerant protein) (hSTP). [Source:Uniprot/SWISSPROT;Acc:Q15642]
9246	UBE2L6	Ubiquitin/ISG15-conjugating enzyme E2 L6 (EC 6.3.2.19) (Ubiquitin- protein ligase L6) (Ubiquitin carrier protein L6) (UbcH8) (Retinoic acid-induced gene B protein) (RIG-B). [Source:Uniprot/SWISSPROT;Acc:O14933]
7374	UNG	Uracil-DNA glycosylase (EC 3.2.2.-) (UDG). [Source:Uniprot/SWISSPROT;Acc:P13051]
9100	USP10	Ubiquitin carboxyl-terminal hydrolase 10 (EC 3.1.2.15) (Ubiquitin thioesterase 10) (Ubiquitin-specific-processing protease 10) (Deubiquitinating enzyme 10). [Source:Uniprot/SWISSPROT;Acc:Q14694]
7375	USP4	Ubiquitin carboxyl-terminal hydrolase 4 (EC 3.1.2.15) (Ubiquitin thioesterase 4) (Ubiquitin-specific-processing protease 4) (Deubiquitinating enzyme 4) (Ubiquitous nuclear protein homolog). [Source:Uniprot/SWISSPROT;Acc:Q13107]

Up-regulated ISGs

Entrez Gene ID	Gene Symbol	Description
25841	ABTB2	Ankyrin repeat and BTB/POZ domain-containing protein 2. [Source:Uniprot/SWISSPROT;Acc:Q8N961]
341	APOC1	Apolipoprotein C-I precursor (Apo-CI) (ApoC-I). [Source:Uniprot/SWISSPROT;Acc:P02654]
716	C1S	Complement C1s subcomponent precursor (EC 3.4.21.42) (C1 esterase) [Contains: Complement C1s subcomponent heavy chain; Complement C1s subcomponent light chain]. [Source:Uniprot/SWISSPROT;Acc:P09871]
440068	CASP1	Caspase-1 precursor (EC 3.4.22.36) (CASP-1) (Interleukin-1 beta convertase) (IL-1BC) (IL-1 beta-converting enzyme) (ICE) (Interleukin- 1 beta-converting enzyme) (p45) [Contains: Caspase-1 p20 subunit; Caspase-1 p10 subunit].
6364	CCL20	Small inducible cytokine A20 precursor (CCL20) (Macrophage inflammatory protein 3 alpha) (MIP-3-alpha) (Liver and activation- regulated chemokine) (CC chemokine LARC) (Beta chemokine exodus-1) [Contains: CCL20(1-67); CCL20(1-64); CCL20(2-70)].
629	CFB	Complement factor B precursor (EC 3.4.21.47) (C3/C5 convertase) (Properdin factor B) (Glycine-rich beta glycoprotein) (GBG) (PBF2) [Contains: Complement factor B Ba fragment; Complement factor B Bb fragment]. [Source:Uniprot/SWISSPROT;Acc:P00751]
80347	COASY	Bifunctional coenzyme A synthase (CoA synthase) (NBP) (POV-2) [Includes: Phosphopantetheine adenylyltransferase (EC 2.7.7.3) (Pantetheine-phosphate adenylyltransferase) (PPAT) (Dephospho-CoA pyrophosphorylase); Dephospho-CoA kinase (EC 2.7.1.24) (DPCK)
1390	CREM	cAMP-responsive element modulator (Inducible cAMP early repressor) (ICER). [Source:Uniprot/SWISSPROT;Acc:Q03060]
6376	CX3CL1	Fractalkine precursor (CX3CL1) (Neurotactin) (CX3C membrane-anchored chemokine) (Small

		inducible cytokine D1). [Source:Uniprot/SWISSPROT;Acc:P78423]
731937	EIF1	Eukaryotic translation initiation factor 1 (eIF1) (Protein translation factor SUI1 homolog) (Sui1iso1) (A121). [Source:Uniprot/SWISSPROT;Acc:P41567]
8334	HIST1H2AC	Histone H2A type 1-C. [Source:Uniprot/SWISSPROT;Acc:Q93077]
3108	HLA-DMA	HLA class II histocompatibility antigen, DM alpha chain precursor (MHC class II antigen DMA). [Source:Uniprot/SWISSPROT;Acc:P28067]
3306	HSPA2	Heat shock-related 70 kDa protein 2 (Heat shock 70 kDa protein 2). [Source:Uniprot/SWISSPROT;Acc:P54652]
3308	HSPA4	Heat shock 70 kDa protein 4 (Heat shock 70-related protein APG-2) (HSP70RY). [Source:Uniprot/SWISSPROT;Acc:P34932]
3397	ID1	DNA-binding protein inhibitor ID-1 (Inhibitor of DNA binding 1). [Source:Uniprot/SWISSPROT;Acc:P41134]
3429	IFI27	Interferon-alpha-induced 11.5 kDa protein (p27) (ISG12(a) protein). [Source:Uniprot/SWISSPROT;Acc:P40305]
3434	IFIT1	Interferon-induced protein with tetratricopeptide repeats 1 (IFIT-1) (Interferon-induced 56 kDa protein) (IFI-56K). [Source:Uniprot/SWISSPROT;Acc:P09914]
24138	IFIT5	Interferon-induced protein with tetratricopeptide repeats 5 (IFIT-5) (Retinoic acid- and interferon-inducible 58 kDa protein). [Source:Uniprot/SWISSPROT;Acc:Q13325]
3665	IRF7	Interferon regulatory factor 7 (IRF-7). [Source:Uniprot/SWISSPROT;Acc:Q92985]
3669	ISG20	Interferon-stimulated gene 20 kDa protein (EC 3.1.13.1) (Promyelocytic leukemia nuclear body-associated protein ISG20) (Estrogen-regulated transcript 45 protein). [Source:Uniprot/SWISSPROT;Acc:Q96AZ6]
4149	MAX	Protein max (Myc-associated factor X). [Source:Uniprot/SWISSPROT;Acc:P61244]
4170	MCL1	Induced myeloid leukemia cell differentiation protein Mcl-1 (Bcl-2- related protein EAT/mcl1) (mcl1/EAT). [Source:Uniprot/SWISSPROT;Acc:Q07820]
8202	NCOA3	Nuclear receptor coactivator 3 (EC 2.3.1.48) (NCoA-3) (Thyroid hormone receptor activator molecule 1) (TRAM-1) (ACTR) (Receptor-associated coactivator 3) (RAC-3) (Amplified in breast cancer-1 protein) (AIB-1) (Steroid receptor coactivator protein 3)
9111	NMI	N-myc-interactor (Nmi) (N-myc and STAT interactor). [Source:Uniprot/SWISSPROT;Acc:Q13287]
8204	NRIP1	Nuclear receptor-interacting protein 1 (Nuclear factor RIP140) (Receptor-interacting protein 140). [Source:Uniprot/SWISSPROT;Acc:P48552]
4938	OAS1	2-5-oligoadenylate synthetase 1 (EC 2.7.7.-) ((2-5)oligo(A) synthetase 1) (2-5A synthetase 1) (p46/p42 OAS) (E18/E16). [Source:Uniprot/SWISSPROT;Acc:P00973]
10133	OPTN	Optineurin (Optic neuropathy-inducing protein) (E3-14.7K-interacting protein) (FIP-2) (Huntingtin-interacting protein HYPL) (NEMO-related protein) (Transcription factor IIIA-interacting protein) (TFIIIA- IntP). [Source:Uniprot/SWISSPROT;Acc:Q96CV9]
51131	PHF11	PHD finger protein 11 (BRCA1 C-terminus-associated protein) (Renal carcinoma antigen NY-REN-34). [Source:Uniprot/SWISSPROT;Acc:Q9UIL8]
51296	SLC15A3	solute carrier family 15, member 3 [Source:RefSeq_peptide;Acc:NP_057666]
8651	SOCS1	Suppressor of cytokine signaling 1 (SOCS-1) (JAK-binding protein) (JAB) (STAT-induced STAT inhibitor 1) (SSI-1) (Tec-interacting protein 3) (TIP-3). [Source:Uniprot/SWISSPROT;Acc:O15524]
3431	SP110	Sp110 nuclear body protein (Speckled 110 kDa) (Transcriptional coactivator Sp110) (Interferon-induced protein 41/75). [Source:Uniprot/SWISSPROT;Acc:Q9HB58]

7128	TNFAIP3	Tumor necrosis factor, alpha-induced protein 3 (EC 3.4.19.12) (Putative DNA-binding protein A20) (Zinc finger protein A20). [Source:Uniprot/SWISSPROT;Acc:P21580]
8717	TRADD	Tumor necrosis factor receptor type 1-associated DEATH domain protein (TNFR1-associated DEATH domain protein) (TNFRSF1A-associated via death domain). [Source:Uniprot/SWISSPROT;Acc:Q15628]
11074	TRIM31	Tripartite motif-containing protein 31. [Source:Uniprot/SWISSPROT;Acc:Q9BZY9]
85363	TRIM5	Tripartite motif-containing protein 5 (EC 6.3.2.-) (RING finger protein 88). [Source:Uniprot/SWISSPROT;Acc:Q9C035]

From the cDNA microarray data of NRAV-overexpressing cells, 107 differentially expressed ISGs were identified by using the Interferome analysis with parameters human, lung and A549 cell line. 72 down-regulated and 35 up-regulated ISGs are shown.

Table S3. Mass Spectrometry Analysis of ZONAB, Related to Figure 6

Reference Scan(s)	Peptide	MH+	DeltaM	z	Type	P (pro) P (pep)	**Score** XC	Coverage DeltaCn
ZO-1–associated nucleic acid binding protein (ZONAB) [Homo sapiens]						1.98E-10	**148.30**	
3768	R.NDTKEDVFVHQTAIKK.N	1874.08736	-0.07095	2	CID	2.05E-07	5.12	0.51
3788	K.EDVFVHQTAIKK.N	1415.61915	-0.29085	2	CID	4.81E-05	3.36	0.36
3831	R.PAPAVGEAEDKENQQATSGPNQPSVR.R	2678.81039	0.20204	3	CID	1.98E-10	3.89	0.43
4062	R.NGYGFINRNDTK.E	1399.49353	-0.85896	2	CID	2.17E-06	3.38	0.44
4171	K.DGVPEGAQLQGPVHR.N	1560.69644	0.80263	2	CID	4.17E-07	3.37	0.52
4194	R.NDTKEDVFVHQTAIK.R	1745.91444	-0.04428	2	CID	5.04E-10	4.95	0.47
4272	K.EDVFVHQTAIK.R	1287.44623	-0.59780	2	CID	1.23E-05	3.32	0.41
4273	K.GAEAANVTGPDGVPVEGSR.Y	1783.87794	1.41825	2	CID	2.77E-03	3.81	0.45
4339	K.VLATKVLGTVK.W	1129.41808	0.17279	2	CID	9.02E-07	3.43	0.43
4384	R.NAGEIGEM*KDGVPEGAQLQGPVHR.N	2506.73309	-0.62057	3	CID	4.77E-07	4.56	0.43
4452	R.NGYGFINR.N	941.02532	-0.10120	2	CID	1.21E-04	2.69	0.43
4928	R.NAGEIGEMKDGVPEGAQLQGPVHR.N	2490.73818	-0.05303	3	CID	4.21E-10	5.93	0.57
5326	R.NGYGFINRNDTKEDVFVHQTAIK.R	2667.91717	0.16020	3	CID	1.05E-09	5.21	0.43
6294	K.VLGTVKWFNVR.N	1319.57943	0.33309	2	CID	1.50E-07	3.27	0.48
8163	R.SVGDGETVEFDVVEGEK.G	1796.86702	0.46457	2	CID	5.01E-07	4.95	0.51

Sequence coverage of ZO-1–associated nucleic acid binding protein (ZONAB)

MSEAGEATTTTTTTLPQAPTEAAAAAPQDPAPKSPVGSGAPQAAAPAPAAHVAGNPGGDAAPAATGTAAAASLATAAGSEDAEKKVLATKVLGTVKWFNVRNGYGFINRNDTKED
VFVHQTAIKKNNPRKYLRSVGDGETVEFDVVEGEKGAEAANVTGPDGVPVEGSRYAADRRRYRRGYYGRRRGPPRNAGEIGEMKDGVPEGAQLQGPVHRNPTYRPRYRSRGPPRP
RPAPAVGEAEDKENQQATSGPNQPSVRRGYRRPYNYRRRPRPPNAPSQDGKEAKAGEAPTENPAPPTQQSSAE

Mass Spectrometry was performed as described in Supplemental Experimental Procedures. Machted peptides were listed or shown in Red.

Supplemental Experimental Procedures

Cells, viruses, and antibodies

Cells A549, HeLa, K562, 293T, HepG2, SMMC-7721, QGY-7703, BEL-7402, NIH3T3, and Vero were grown in DMEM or RPMI1640 supplemented with 10% (vol/vol) FBS (Gibco) and antibiotics (penicillin and streptomycin) (Invitrogen) at 37 ℃ in a humidified 5% CO_2 atmosphere as previously described (Guo et al., 2010). Influenza virus A/WSN/33 (H1N1) and Sendai virus (SeV) were propagated in embryonated chicken eggs (Wei et al., 2014). Muscovy Duck Reovirus (MDRV) and Herpes simplex virus (HSV, kindly provided by Prof. Jinhua Yan, Institute of Microbiology, Chinese Academy of Sciences (Zhang et al., 2011)) were propagated in Vero cells. Antibody anti-MxA (Proteintech, 13750-1-AP) is used for Western blot. All other antibodies were obtained as previously described (Wei et al., 2014).

Plasmid construction

The reporter plasmid pGL3-MxAP-FF-Luc carrying the firefly luciferase (FFLuc) gene under the control of the human MxA promoter was kindly provided by Prof. Georg Kochs, Department of Virology, University of Freiburg, Freiburg, Germany (Holzinger et al., 2007). Primers ′5 -TTA AAA GGT ACC GAG CCC TGA ACC GGG ACA GTG-3′ and 5′-TTT GTC AAG CTT TGG TGT CCA GCG AAG ACC AGC-3′ were used to amplify the IFITM3 promoter from A549 genomic DNA (Shen et al., 2013). pGL3-IFITM3P carrying the FF-Luc gene under the control of the IFITM3 promoter was constructed by inserting the IFITM3 promoter into the

XhoI-HindIII sites of pGL3-basic (Promega).

Viral infection

A549 cells were used to infect with IAV WSN, Sendai virus (SeV), or Herpes Simplex Virus (HSV) and 293T cells were infected with Muscovy Duck Reovirus (MDRV). Unless indicated, cells were washed and incubated with virus at a multiplicity of infection (MOI) of 3 for 1 h with medium containing 2 mg/ml TPCK (L-1-tosylamido-2-phenylethyl chloromethyl ketone) -treated trypsin. After adsorption, the supernatant was aspirated and cells were cultured with the medium for 12 h with IAV WSN and SeV, or 24h with MDRV and HSV.

Virus titers assay

Cell culture supernatant was harvested at 16 hpi or indicated time points. Mouse lungs were collected at 6 dpi and homogenized in 1ml DMEM to prepare tissue suspension. Virus titers in supernatants were determined by a standard Hemagglutination assay (HA) or a plaque forming assay (PFU) on MDCK cells as described previously (Wang et al., 2012).

Microarray and data analysis

The microarray experiments were performed as described previously (Guo et al., 2014; Wang et al., 2012). The lncRNA microarray of WSN infected A549 cells and uninfected control was performed using Human lncRNA 100309 (Arraystar,

Rockville, MD). The cDNA microarray of WSN infected NRAV-overexpressing or control A549 cells (MOI=3,16 hpi).was performed using Human 12x135K microarray (Roche NimbleGen, Madison, WI). Expression data were normalized through quantile normalization and the Robust Multichip Average (RMA) algorithm, and transformed into log2 value for calculation. The fold changes of up-regulated genes are calculated as $2^{(\text{mean}[\log2(T1),\ \log2(T2),\ \log2(T3)])}/2^{(\text{mean}[\log2(C1),\ \log2(C2),\ \log2(C3)])}$, and the fold changes of down-regulated genes are calculated as $2^{(\text{mean}[\log2(C1),\ \log2(C2),\ \log2(C3)])}/2^{(\text{mean}[\log2(T1),\ \log2(T2),\ \log2(T3)])}$. Differentially expressed genes were identified through Volcano Plot filtering between two groups, and the threshold is fold change > 2.0 and $P<0.05$. In heatmaps, log2 values have been centered and scaled in the row.

***In Silico* and Primary Functional Screen of LncRNAs**

To identify lncRNAs from the data of microarray, candidates with higher fold change of expression were selected and subjected an *in silico* analysis of genomic locations and sequences (UCSC, http://genome.ucsc.edu, NCBI, http://www.ncbi.nlm.nih.gov), and according to the strict criteria that lncRNA should be longer than 200 nt, have little or no ORFs, and localize in genome antisense to, or intronic of, or intergenic (>5kb away) from adjacent protein-coding genes. No protein-coding potential is performed. The functional primary screen is based on the effects of ectopic lncRNA expression on IAV replication. Fragments of lncRNAs amplified from A549 cell were inserted into modified stable expression system as described in **Supplemental Experimental Procedures** and used for exogenous expression. FACS sorted cells

with fluorescence are maintained. After infection with WSN at MOI=0.3 for 16 hours, the virus titers in cell culture supernatants were determined through plaque forming assay.

Bioinformatics analysis of non-coding potential

Non-coding potential is performed through several programs as described previously (Guo et al., 2014). LncRNA sequences are analyzed by using ORF Finder from NCBI (http://www.ncbi.nlm.nih.gov/gorf/gorf.html) and coding potential calculator (http://cpc.cbi.pku.edu.cn). NRAV homolog sequences from human, chimpanzee, rhesus, guenin pig, and mouse are used for PhyloCSF analysis (Lin et al., 2011) (https://github.com/mlin/PhyloCSF/wiki).

Sucrose sedimentation and polysome analysis

The sucrose sedimentation and polysome analysis was performed as previously described (Carpenter et al., 2013; Ricci et al., 2014). 2×10^7 A549 cells were pretreated with cycloheximide (CHX, 100 μg/ml, Sigma) for 10 min at 37℃ or mock treated. After wash, cells were lysed in 1ml of lysis buffer (10mM HEPES-KOH pH 7.4; 5 mM $MgCl_2$; 300 mM KCl; 0.5% NP-40; 2mM DTT; 100 μg/ml CHX (none for control) and 1 × Protease-Inhibitor Cocktail EDTA-free (Promega)) and incubation at 4ºC for 10 min. After centrifugation at 1300 g for 10 min at 4ºC, the supernatant was recovered. 10 A260 units of mock lysate were treated with 35 mM of EDTA for 20 min, same amount of CHX-treated lysate were not complemented with EDTA, both

were loaded on top of a 10 to 50% (Weight/Volume) sucrose gradient (20mM HEPES-KOH pH 7.4; 5mM $MgCl_2$; 100mM KCl; 2mM DTT; 100 µg/ml CHX) and centrifuged in a SW-41 rotor at 35,000 rpm for 2 h 40 min at 4 ºC. After centrifugation, 15 fractions were collected from the top while absorbance at 254nm was measured. Collected fractions were digested with 1% SDS and proteinase K (200 µg/ml) at 42C for 30 min. RNA was extracted and re -suspended in 50 µl of water. qRT-PCR was performed to quantify the NRAV or GAPDH mRNA distribution in sucrose gradient. The relative RNA levels were normalized to input and shown as %input.

Cell stimulation, Transient transfections and viral transductions

For stimulation, cells were incubated for 2-3 h with the recombinant cytokines or peptides at following concentration IFN-β (0-100 ng/ml), IL-29 (50 ng/ml), for 8 h with LPS (100 ng/ml, Invivogen) and sCD14 (300 ng/ml, PeproTech), for 4 h with etoposide (100 µM, Sigma), or cultured in serum-free media, or transfected with 1 µg/ml RNA or poly(I:C) using Lipofectamine 2000 (Invitrogen) according to the manufacturer's instructions. For transient transfection, cells were transiently transfected with 2 µg plasmids per well of 6-well plate by using Lipofectamine 2000 (Invitrogen). Then, cells were cultured for another 24 hours for transient expression. For viral transductions, cells were transduced with pseudovirus packaged by lentivirus expression system with polybrene (8 µg/ml).

RT-PCR and Quantitative RT-PCR (qRT-PCR)

RNA was isolated with the Total RNA Kit (Omega Bio-Tek). Reverse transcription was performed with oligo-dT primers or random primers by using M-MLV (Promega), and quantitative PCR was performed with SuperReal PreMix Plus (SYBR Green) (Tiangen, Beijing, China). The primer sequences are available upon request. For quantification, the $2^{-\Delta\Delta Ct}$ method was used to calculate the relative RNA levels against GAPDH. Results from three independent experiments were expressed as means ± s.e.m. $P<0.05$ (two-sided Student's *t*-test) was considered statistically significant.

shRNAs

The shRNA target sequences used in supplemental results are sh-RIG-I: TGC AAT CTT GTC ATC CTT TAT (Jiang et al., 2011), sh-MDA5: CCA ACA AAG AAG CAG TGT ATA (Delaloye et al., 2009), sh-TLR3: CAA CAT AGC CAA CAT AAA T (Salaun et al., 2007), sh-VISA: GGC AGG TCA GTT AAC AAT TTA (Jiang et al., 2011), sh-IRF3: CAT TGT AGA TCT GAT TAC CTT C (Manel et al., 2010), sh-IRF7: GCC TCT ATG ACG ACA TCG AGT, sh-STAT1: GCA AGC GTA ATC TTC AGG ATA (Jiang et al., 2011) and sh-ZONAB: GCA GGT GAC CTA AAG AAT TAA and GGA AGA CTA ACC AAG ATT TG. The efficiency of overexpression or knockdown was confirmed by standard RT-PCR or qRT-PCR.

Generation of overexpression and knockdown cell lines

NRAV coding sequence and other lncRNA sequences were cloned from A549 by

RT-PCR. Primers were designed according to the sequences in database of UCSC (http://genome.ucsc.edu) or NCBI (http://www.ncbi.nlm.nih.gov). The stable NRAV-overexpressing cells lines were constructed with a retroviral expression system as described previously (Qiu et al., 2012; Wei et al., 2014; Yang et al., 2013). The expression construct is modified by inserting a bovine growth hormone polyadenylation (BGH-polyA) sequence from pcDNA3.1 into XhoI-EcoRI sites before the GFP coding sequence in the vector. The stable knockdown cells of NRAV were generated using a shRNA-based lentivector system pSIH-H1 (System Biosciences) as provider's protocol. The shRNA target sequences used in this paper are sh-NRAV-1: GCC CTT CAG AGT TGT TAC T, sh-NRAV-2: CCT CCG AAC AGA GTA ATG T. The efficiency of overexpression or knockdown was confirmed by standard RT-PCR or qRT-PCR.

Transgenic mice and virus challenge

The NRAV transgenic C57BL/6 mice (TG) were created as previously described (Lu et al., 2012; Wang et al., 2014; Wei et al., 2014). The NRAV genotype was verified by PCR. The NRAV expression was determined by RT-PCR of mouse tissue after euthanasia. Transgenic lines with high expression were maintained and used in this study. The C57BL/6 wild-type (WT) and NRAV-expressing TG mice (5–6 weeks of age, 5-13 mice/group) were inoculated intranasally with or without 10^3 PFU (about $0.5\times LD_{50}$ for WT mice) of WSN diluted in 50 μL of sterile phosphate buffer saline (PBS). Mice were weighted daily to monitor signs of illness for a period of 14 days.

Mouse lungs (13 mice/group) were collected on 6 dpi and used for further examination. Lung viral loads were measured by standard plaque forming assay, and mouse ISGs mRNA levels in lung were quantified by real-time RT-PCR and RT-PCR. Haematoxylin and Eosin (HE) staining of mouse lung was performed as previously described (Wang et al., 2014).

ISGs transient expression experiment

The transient expression of exogenous human IFIT2, IFIT3, IFITM3 and MxA were performed on NRAV-overexpressing and EV cells by transfecting with plasmids of these ISGs (1 μg/well in 6-well plate) for 24 hours, and followed with IAV infection for 16 hours. The relative virus titer (% of control EV cells) in the culture supernatant of NRAV cells and EV cells was calculated based on the virus titers determined by plaque forming assay. The empty transient expression plasmid was used as control, as well as the expression plasmid of DDX3X. The transient expression efficiency was determined by RT-PCR 24 hours after transfection with expression plasmid containing the coding sequence.

Subcellular fractionation

Cytoplasmic and nuclear fractions were separated as described previously (Yoon et al., 2012). Briefly, A549 cells were lysed with TD buffer (25 mM Tris-HCl pH 7.4; 100 mM NaCl; 5 mM KCl; and 0.7mM Na_2HPO_4) containing 1% NP-40 for 5 min. The lysates were centrifuged with 12,000 rpm for 5 min at 4ºC. The supernatant was

collected and used for the cytoplasmic fraction. The nuclear pellets were washed with TD buffer containing 0.5% NP-40 on ice for 5 min and collected after centrifugation at 4ºC for 5 min at 12,000 rpm.

Luciferase assay

Luciferase assay was performed as previously described (Wei et al., 2014). Briefly, 293T cells stably expressing NRAV in 24-well plate were cotransfected with 0.8μg of pGL3-MxAP or pGL3-IFITM3P, and 30ng of a Renilla luciferase plasmid (pRL-TK, Promega). Luciferase activity was measured using the dual-luciferase reporter assay system according to the manufacturer's instruction (Promega).

5-Aza-2'-deoxycytidine treatment

Cells were treated with or without 10 μM DNA methyltransferase inhibitor 5-Aza-2'-deoxycytidine (decitabine; DAC, Sigma) for 2 days, and supplemented with fresh DAC every 24h. Treated cells were infected with virus (WSN, SeV, MDRV or HSV, MOI=3) for 12 ~ 24 h. RNAs were isolated using Trizol reagent (Tiangen, Beijing, China), reverse transcription were performed using oligo-dT primers and mRNA levels were detected by RT-PCR or qRT-PCR.

RNA stabilization assays

The mRNA expression of MxA in A549 cells were induced by infection with WSN at MOI=1 for 12 h. The infected cells were treated with actinomycin D (ActD, Sigma) at

2.5 μg/ml and collected at 0, 4, 12, 20 h time points. RNAs were extracted using Trizol reagent (Tiangen, Beijing, China), reverse transcription were performed using oligo-dT primers and mRNA levels were determined by RT-PCR or qRT-PCR.

Chromatin immunoprecipitation (ChIP)

A549 cells expressing NRAV or EV control were infected with WSN (MOI=1, 12 hpi) and were subjected to ChIP assays using the Magna ChIP A/G chromatin immunoprecipitation kit (Millipore) following the manufacturer's instruction. Briefly, 10^7 cells were fixed and lysed in 500μl lysis buffer. Nucleus fraction were pelleted and resuspended in 300 μl nucleus lysis buffer, followed by sonication. Sheared chromatin was immunoprecipitated with 3 μg anti-H3K4me3 (Millipore; 17-614), anti-H3K27me3 (Millipore; 07-449) or IgG control (Millipore) antibody and 20μl magentic beads at 4°C for 4 h to overnight. To reverse the cross-links, protein digestion with proteinase K and 0.2 M NaCl were performed. Immunoprecipitated DNA was purified and quantified by qPCR analysis using SYBR Green Supermix (Tiangen). Primers used locate in intron3-exon4 of *mxA* (transcription start site for MxA isoform 2) and exon1 of *ifitm3*. The primer sequences used for the *mxA* gene are 5' CCG AGC TGG GCA ATT GG 3' and 5' TCC TGG CCG GCA ACT G 3'), for *ifitm3* are 5' AAA GGG AGG GCT CAC TGA GAA 3' and 5' CAC CTC GTG CTC CTC CTT GA 3', for *gapdh* are 5' TAC TAG CGG TTT TAC GGG CG 3' and 5' TCG AAC AGG AGG AGC AGA GAG CGA 3', for *dynll1* are 5' GAG CCC GGT CTC ACC GTG GA 3' and 5' GAT GCG CCA CGG CTT CGG TA 3' (Jurado et al.,

2012). Modificated histone enrichment in the ChIP samples were normalized to the input DNA and was calculated as $2^{-\Delta\Delta Ct}$ with normalization against IgG control. Experiments were performed at least three times with independent chromatin samples.

RNA pull-down assay and *Mass Spectrometry*

Three pairs of antisense DNA probes of 20-30 bp binding with NRAV and scramble probes were synthesized and labeled with biotin. 10^8 uninfected A549 cells were lysed in 7ml ice-cold IP Lysis buffer (25mM Tris-HCl pH 7.4; 150mM NaCl; 1mM EDTA; 1% NP-40 and 5% glycerol) complemented with 1 × Protease-Inhibitor Cocktail EDTA-free (Promega) and 7μl of Ribolock RNase inhibitor (Thermo) and incubated on ice for 30min. Supernatant of lysates were incubated with 0.5 nmole of NRAV antisense probes or scramble control probes for 3 h at 4℃ followed by incubation with Streptavidin Dynabeads (Invitrogen) overnight. RNA/protein interacting complexes were immunoprecipated and visualized by silver-staining (Pierce silver stain kit, Thermo). Specific bands were excised and trypsin digested. LC-MS/MS analysis was performed using a ThermoFisher Finnigan LTQ linear ion trap Mass Spectrometer in line with a ThermoFisher Finnigan Survey or MS Pump Plus HPLC system (Beijing Regional center of life science instrument, Chinese Academy of Sciences). The raw MS data were analyzed using SEQUEST v.28 against NCBI human protein database and results were filtered, sorted, and displayed using the Bioworks 3.2.

RNA immunoprecipitation (RIP)

2×10^7 uninfected A549 cells were lysed in 200 µl of ice-cold IP lysis buffer as described in RNA pull-down assay. Lysate was 5 to 10-fold diluted in 1ml RIP buffer (25 mM Tris-HCl pH 7.4; 150mM KCl; 5mM EDTA; 0.5 mM DTT; 0.5% NP-40; 100U/ml RNase inhibitor (Thermo) and 1 × Protease-Inhibitor Cocktail EDTA-free (Promega)) and incubated with 10 µg anti-ZONAB antibody (Bioss, Beijing) or rabbit IgG control (Millipore) overnight at 4°C as previously described (Tsai et al., 2010). Lysate was then incubation with Protein A Dynabeads (Invitrogen) for 3 h at 4°C. RNA/protein complexes were immunoprecpitated and RNA was extracted and measured with qRT-PCR.The relative RNA levels were normalized to input and the fold enrichment was calculated as $2^{-\Delta\Delta Ct}$ with normalization to IgG control.

Predition of CpG island and transcription factor binding

The prediction data of CpG island in NRAV promoter region and binding sites of transcription factors were from UCSC genome browser database (February 2009 human reference sequence (GRCh37)) (Karolchik et al., 2014).

Supplemental References

Delaloye, J., Roger, T., Steiner-Tardivel, Q.G., Le Roy, D., Knaup Reymond, M., Akira, S., Petrilli, V., Gomez, C.E., Perdiguero, B., Tschopp, J*., et al.* (2009). Innate immune sensing of modified vaccinia virus Ankara (MVA) is mediated by TLR2-TLR6, MDA-5 and the NALP3 inflammasome. PLoS pathogens *5*, e1000480.

Guo, G., Qiu, X., Wang, S., Chen, Y., Rothman, P.B., Wang, Z., Chen, Y., Wang, G., and Chen, J.L. (2010). Oncogenic E17K mutation in the pleckstrin homology domain of AKT1 promotes v-Abl-mediated pre-B-cell transformation and survival of Pim-deficient cells. Oncogene *29*, 3845-3853.

Holzinger, D., Jorns, C., Stertz, S., Boisson-Dupuis, S., Thimme, R., Weidmann, M., Casanova, J.L., Haller, O., and Kochs, G. (2007). Induction of MxA gene expression by influenza A virus requires type I or type III interferon signaling. Journal of virology *81*, 7776-7785.

Jiang, L.J., Zhang, N.N., Ding, F., Li, X.Y., Chen, L., Zhang, H.X., Zhang, W., Chen, S.J., Wang, Z.G., Li, J.M*., et al.* (2011). RA-inducible gene-I induction augments STAT1 activation to inhibit leukemia cell proliferation. Proceedings of the National Academy of Sciences of the United States of America *108*, 1897-1902.

Jurado, S., Conlan, L.A., Baker, E.K., Ng, J.L., Tenis, N., Hoch, N.C., Gleeson, K., Smeets, M., Izon, D., and Heierhorst, J. (2012). ATM substrate Chk2-interacting Zn2+ finger (ASCIZ) Is a bi-functional transcriptional activator and feedback sensor in the regulation of dynein light chain (DYNLL1) expression. The Journal of biological chemistry *287*, 3156-3164.

Karolchik, D., Barber, G.P., Casper, J., Clawson, H., Cline, M.S., Diekhans, M., Dreszer, T.R., Fujita, P.A., Guruvadoo, L., Haeussler, M*., et al.* (2014). The UCSC Genome Browser database: 2014 update. Nucleic acids research *42*, D764-770.

Lu, D., Ma, Y., Zhang, W., Bao, D., Dong, W., Lian, H., Huang, L., and Zhang, L. (2012). Knockdown of cytochrome P450 2E1 inhibits oxidative stress and apoptosis in the cTnT(R141W) dilated cardiomyopathy transgenic mice. Hypertension *60*, 81-89.

Manel, N., Hogstad, B., Wang, Y., Levy, D.E., Unutmaz, D., and Littman, D.R. (2010). A cryptic sensor for HIV-1 activates antiviral innate immunity in dendritic cells. Nature *467*, 214-217.

Qiu, X., Guo, G., Chen, K., Kashiwada, M., Druker, B.J., Rothman, P.B., and Chen, J.L. (2012). A requirement for SOCS-1 and SOCS-3 phosphorylation in Bcr-Abl-induced tumorigenesis. Neoplasia *14*, 547-558.

Ricci, E.P., Kucukural, A., Cenik, C., Mercier, B.C., Singh, G., Heyer, E.E., Ashar-Patel, A., Peng, L., and Moore, M.J. (2014). Staufen1 senses overall transcript secondary structure to regulate translation. Nature structural & molecular biology *21*, 26-35.

Salaun, B., Lebecque, S., Matikainen, S., Rimoldi, D., and Romero, P. (2007). Toll-like receptor 3 expressed by melanoma cells as a target for therapy? Clinical cancer research : an official journal of the American Association for Cancer Research *13*, 4565-4574.

Shen, C., Wu, X.R., Jiao, W.W., Sun, L., Feng, W.X., Xiao, J., Miao, Q., Liu, F., Yin, Q.Q., Zhang, C.G*., et al.* (2013). A functional promoter polymorphism of IFITM3 is associated with susceptibility to pediatric tuberculosis in Han Chinese population. PloS one *8*, e67816.

Tsai, M.C., Manor, O., Wan, Y., Mosammaparast, N., Wang, J.K., Lan, F., Shi, Y., Segal, E., and Chang, H.Y. (2010). Long noncoding RNA as modular scaffold of histone modification complexes. Science *329*, 689-693.

Wang, S., Li, H., Chen, Y., Wei, H., Gao, G.F., Liu, H., Huang, S., and Chen, J.-L. (2012). Transport of

influenza virus neuraminidase (NA) to host cell surface is regulated by ARHGAP21 and Cdc42 proteins. Journal of Biological Chemistry *287*, 9804-9816.

Yang, J., Wang, J., Chen, K., Guo, G., Xi, R., Rothman, P.B., Whitten, D., Zhang, L., Huang, S., and Chen, J.L. (2013). eIF4B phosphorylation by Pim kinases plays a critical role in cellular transformation by Abl oncogenes. Cancer research *73*, 4898-4908.

Yoon, J.H., Abdelmohsen, K., Srikantan, S., Yang, X., Martindale, J.L., De, S., Huarte, M., Zhan, M., Becker, K.G., and Gorospe, M. (2012). LincRNA-p21 suppresses target mRNA translation. Molecular cell *47*, 648-655.

Zhang, N., Yan, J., Lu, G., Guo, Z., Fan, Z., Wang, J., Shi, Y., Qi, J., and Gao, G.F. (2011). Binding of herpes simplex virus glycoprotein D to nectin-1 exploits host cell adhesion. Nature communications *2*, 577.